ORGANOMETALLICS

Article

pubs.acs.org/Organometallics

The Reductive Activation of CO_2 Across a Ti═Ti Double Bond: Synthetic, Structural, and Mechanistic Studies

Alexander F. R. Kilpatrick,[†] Jennifer C. Green,*[,‡] and F. Geoffrey N. Cloke*[,†]

[†]Department of Chemistry, School of Life Sciences, University of Sussex, Brighton BN1 9QJ, U.K.

[‡]Department of Chemistry, University of Oxford, Inorganic Chemistry Laboratory, South Parks Road, Oxford OX1 3QR, U.K.

Supporting Information

ABSTRACT: The reactivity of the bis(pentalene)dititanium double-sandwich compound $Ti_2Pn^{\dagger}_2$ (**1**) ($Pn^{\dagger}$ = 1,4-$\{Si^iPr_3\}_2C_8H_4$) with CO_2 is investigated in detail using spectroscopic, X-ray crystallographic, and computational studies. When the CO_2 reaction is performed at −78 °C, the 1:1 adduct **4** is formed, and low-temperature spectroscopic measurements are consistent with a CO_2 molecule bound symmetrically to the two Ti centers in a μ:η^2,η^2 binding mode, a structure also indicated by theory. Upon warming to room temperature the coordinated CO_2 is quantitatively reduced over a period of minutes to give the bis(oxo)-bridged dimer **2** and the dicarbonyl complex **3**. In situ NMR studies indicated that this decomposition proceeds in a stepwise process via monooxo (**5**) and monocarbonyl (**7**) double-sandwich complexes, which have been independently synthesized and structurally characterized. **5** is thermally unstable with respect to a μ-O dimer in which the Ti−Ti bond has been cleaved and one pentalene ligand binds in an η^8 fashion to each of the formally Ti^{III} centers. The molecular structure of **7** shows a "side-on" bound carbonyl ligand. Bonding of the double-sandwich species Ti_2Pn_2 (Pn = C_8H_6) to other fragments has been investigated by density functional theory calculations and fragment analysis, providing insight into the CO_2 reaction pathway consistent with the experimentally observed intermediates. A key step in the proposed mechanism is disproportionation of a mono(oxo) di-Ti^{III} species to yield di-Ti^{II} and di-Ti^{IV} products. **1** forms a structurally characterized, thermally stable CS_2 adduct **8** that shows symmetrical binding to the Ti_2 unit and supports the formulation of **4**. The reaction of **1** with COS forms a thermally unstable complex **9** that undergoes scission to give mono(μ-S) mono(CO) species **10**. Ph_3PS is an effective sulfur transfer agent for **1**, enabling the synthesis of mono(μ-S) complex **11** with a double-sandwich structure and bis(μ-S) dimer **12** in which the Ti−Ti bond has been cleaved.

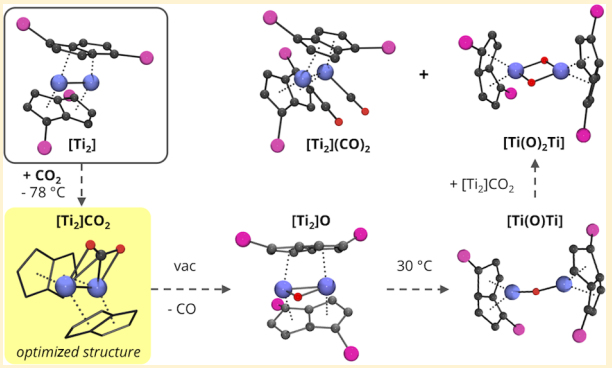

INTRODUCTION

In light of increasing global energy demands and environmental concerns over anthropogenic climate change,[1] there is considerable interest in the utilization of CO_2 as a renewable C_1 feedstock for industrially important chemicals.[2−4] One of the most promising methods is the use of transition-metal catalysts to bring about selective and energy-efficient CO_2 incorporation into organic compounds or reduction to CO, which can then be converted into liquid fuels via Fischer−Tropsch chemistry.[5]

The difficulty in achieving CO_2 reduction lies in the thermodynamic stability of the CO_2 molecule and the kinetic barrier to its activation. As a result, highly reducing oxophilic metal complexes are typically employed. Stoichiometric CO_2 activation has been achieved using well-defined complexes of the main-group and transition metals[6−10] as well as metal-free systems based on frustrated Lewis pairs (FLPs).[11−13] Lower-oxidation-state f-element complexes are also being increasingly explored in this context: for example, Evans and co-workers have shown that samarium(II) metallocenes facilitate the reductive coupling of CO_2 to form oxalate $[O_2CCO_2]^{2-}$ [14,15] and the reductive disproportionation of COS to $[S_2CO]^{2-}$ and CO.[15] More recently, organouranium(III) complexes have attracted interest because of their significant capacity for CO_2 activation.[16−18] For example, trivalent uranium metallocenes $U(Cp^R)_3$ reductively activate CO_2 (for $Cp^R = \eta^5$-$C_5H_4\{SiMe_3\}$) and COS (for $Cp^R = \eta^5$-C_5H_4Me) to generate μ-oxo/μ-sulfido products with concomitant release of CO.[19,20] Density functional theory (DFT) studies by Maron and co-workers have provided insight into the mechanism of reductive CO_2 and COS activation at Sm(II)[21] and U(III)[22,23] centers, implicating in each case a bimetallic μ-CO_2 complex in which carbon dioxide was doubly reduced. The possibility of a concerted pathway involving a monometallic CO_2 intermediate with a $[CO_2]^{\bullet-}$ radical anion ligand was ruled out on the basis of the observed products. Meyer and co-workers reported the first example of a linearly coordinated $[CO_2]^{\bullet-}$ moiety in a U(III)

Received: April 28, 2015
Published: July 4, 2015

DOI: 10.1021/acs.organomet.5b00315
Organometallics 2015, 34, 4816−4829

complex supported by a stabilizing macrocyclic ligand, thus illustrating the importance of ligand architecture in reactivity.[24] Recent studies by Cloke and co-workers with the mixed-sandwich U(III) complexes $(COT')UCp^{Me4R}\{THF\}_x$ (COT' = η^8-1,4-$\{SiMe_3\}_2C_8H_6$; R = Me, Et, ^{i}Pr, ^{t}Bu) have shown that the steric environment around the metal center plays a key role in guiding the possible reductive transformation pathways of CO_2, i.e., reductive coupling, disproportionation, or deoxygenation.[25] Nonetheless, better understanding of the mechanisms of these reductive transformations is required, with a view to tuning the structure of the active complex or the reaction conditions to give more useful product outcomes and assessing the potential for catalytic turnover.[26]

Divalent titanium sandwich complexes are an underdeveloped series of compounds in this regard, despite the rich and varied reaction chemistry that "titanocenes" have shown with a variety of small molecules.[27,28] Alt et al.[29] reported the synthesis of the titanium CO_2 adduct $Cp_2Ti(CO_2)(PMe_3)$ via simple ligand substitution of $Cp_2Ti(PMe_3)_2$, and a number of acetylene complexes of Cp_2Ti have shown CO_2 insertion into the Ti−C bond of the titanacyclopropene ring.[30−33] In contrast, reaction of the permethyltitanocene complex $Cp^*_2Ti(\eta^2\text{-}Me_3SiC_2SiMe_3)$ with CO_2 yields, after elimination of the silylalkyne, a mixture of the dimeric carbonate $(Cp^*_2Ti)_2(CO_3)$ and the carbonyl complex $Cp^*_2Ti(CO)_2$.[34,35] Reductive disproportionation of CO_2 has been achieved by $Cp_2Ti(CO)_2$ to generate CO and the carbonate-bridged tetranuclear complex $[(Cp_2Ti)_2(CO_3)]_2$.[36] Titanium(III) complexes have also shown efficacy in reductive transformations of CO_2 to yield oxo,[36] carbonate,[36−39] and oxalate[40] products, and the relative cheapness and low toxicity of this metal makes it attractive for fundamental reactivity studies.

Multiple bonds between metal atoms have fascinated chemists for over 50 years,[41] and M−M bonded complexes have also shown ability to facilitate the reductive activation of CO_2. Recent examples include systems featuring reduced Mg−Mg,[42] Cr−Cr,[43] and Pd−Pd cores[44] and a highly polar heterobimetallic Zr−Co complex recently reported by Thomas and co-workers.[45]

Our interest in M−M interactions is focused on the aromatic ligand pentalene (Pn, C_8H_6), which is related to Cp by the edge-sharing ring fusion of two cyclopentadienyl fragments and shows a unique variety of coordination modes in its organometallic complexes.[46] In particular, the ability of Pn to bind two metal centers with η^5 hapticity has proven ideal for the synthesis of bimetallic analogues of the ubiquitious bis(Cp)metallocenes, so-called "double-sandwich" complexes.[47−53] We have recently reported the synthesis and characterization of the titanium double-sandwich complex $Ti_2(\mu\text{:}\eta^5,\eta^5\text{-}Pn^\dagger)_2$ (**1**) using the silylated pentalene ligand 1,4-$\{Si^iPr_3\}_2C_8H_4$ ($Pn^\dagger$). In addition to providing a rare example of a Ti−Ti multiple bond, **1** exhibits a solid-state structure unique among the M_2Pn_2 complexes in which the pentalene ligands are nonparallel and tilted around the Ti_2 core.[54] DFT studies on the model system Ti_2Pn_2 calculated an M−M bond order of 2 and an optimized geometry with C_{2v} molecular symmetry, providing a relatively open structure in which the frontier orbitals are sterically accessible.

The combination of a low-valent group IV metal and a metal−metal double-bonded system led us to explore the reactivity of **1** with small molecules. We recently communicated the room-temperature reaction of **1** with 1 equiv of CO_2 to give the bis(oxo)-bridged dimer $[(\eta^8\text{-}Pn^\dagger)Ti(\mu\text{-}O)]_2$ (**2**), in which the Ti−Ti bond has been cleaved, and the dicarbonyl complex $Ti_2(\mu\text{:}\eta^5,\eta^5\text{-}Pn^\dagger)_2(CO)_2$ (**3**), which was independently synthesized from **1** with 2 equiv of CO.[55] Herein we explore the scope of this reductive transformation of CO_2, investigating its mechanistic pathway by the identification of key intermediates using spectroscopic and computational techniques. Furthermore, by the use of isoelectronic CS_2 and unsymmetrical COS as model molecules, we report the isolation and structural characterization of stable analogues for the proposed reaction intermediates, supporting the theoretical predictions. In the interests of brevity, an in-depth description of the bonding in these molecules and other related compounds is provided in the companion paper.[56]

RESULTS

Reaction of CO_2 with $Ti_2Pn^\dagger_2$. The reaction of **1** with 1 equiv of either $^{12}CO_2$ or $^{13}CO_2$ was carried out in methylcyclohexane-d_{14} (MeCy-d_{14}) at −78 °C (Scheme 1).

Scheme 1. Reactivity of 1 with CO_2 (R = Si^iPr_3)

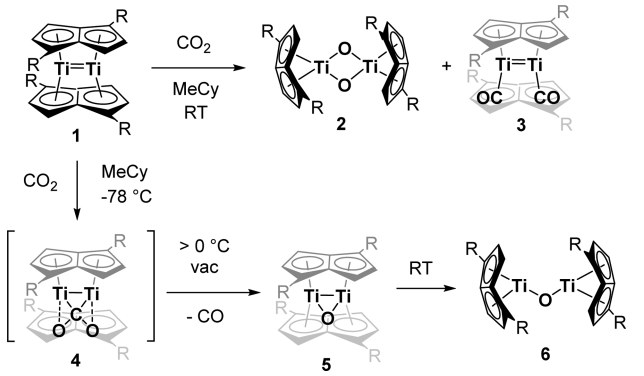

This resulted in a color change from deep red to dark green, which accompanied quantitative conversion of **1** to an intermediate species, **4**, that was observed by low-temperature spectroscopic measurements but had not been previously detected in a room-temperature reaction. The ^{1}H NMR spectrum of **4** at −30 °C showed four sharp doublets in the aromatic region, consistent with a diamagnetic complex that exhibits C_2 molecular symmetry on the NMR time scale, while the $^{13}C\{^1H\}$ spectrum showed a singlet at 219 ppm with no further labeled ^{13}C signals. In situ IR studies of **4** at −65 °C showed distinct bands at 1678 and 1236 cm^{-1}, which shifted to 1637 and 1217 cm^{-1}, respectively, in the isotopically labeled [^{13}C]**4**. These IR bands are assigned to asymmetric and symmetric ν(OCO) stretches, respectively, of the CO_2 ligand by analogy with the monomeric complex $Cp_2Ti(CO_2)(PMe_3)$,[29] which was studied in-depth by Mascetti et al.[57] and shows a C-coordinated bonding mode. Compound **4** could not be isolated because of its susceptibility to further reaction.

When **4** was allowed to warm from −78 °C to ambient temperature under dynamic vacuum, the red mono(oxo) complex **5** was isolated (Scheme 1). **5** could also be obtained by the slow addition of 1 equiv of N_2O to **1** via Toepler line. The ^{1}H NMR spectrum of **5** is again consistent with a diamagnetic complex with C_2 symmetry, and elemental analysis and mass spectrometry measurements support the proposed formulation. The molecular structure determined by single-crystal X-ray diffraction (XRD) reveals a "dimetallaepoxide"

DOI: 10.1021/acs.organomet.5b00315
Organometallics 2015, 34, 4816−4829

structure with an oxo ligand symmetrically bridging two formally Ti(III) centers (Figure 1). The $Pn^{\dagger}$ ligands are less

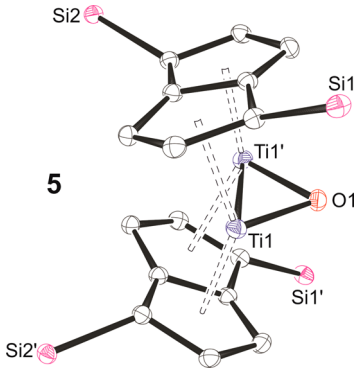

Figure 1. Displacement ellipsoid plot (30% probability) of **5** with hydrogen atoms and ^{i}Pr groups omitted for clarity. Primed atoms are generated by symmetry.

tightly bound to the Ti_2 core of **5** relative to **1** and show the largest average Ti−C and Ti−centroid distances among all of the double-sandwich derivatives structurally characterized herein (Table 1). Interestingly, the ring slippage parameter (Δ = 0.15) and the twist angle between the $Pn^{\dagger}$ ligands and the dimetal unit (26.6(5)°) also have the largest values among all of these structures (see Figure 2 for definitions of these parameters).

Complex **5** is thermally sensitive, and allowing a C_6D_6 solution to stand for 12 h at room temperature led to the precipitation of green crystals of **6**. X-ray crystallography established the connectivity in **6** as a μ-O dimer in which the Ti−Ti bond has been cleaved and one pentalene ligand binds in an η^8 fashion to each of the formally Ti(III) centers (see Scheme 1 and Figure S1 in the Supporting Information). However, the low quality of the X-ray data precludes meaningful discussion of the metric parameters. In the ^{1}H NMR spectrum of **6** in THF-d_8 solution, only broad signals were observed, and the effective magnetic moment determined by the Evans method[58,59] was 1.73μ_B per Ti, a value consistent with one unpaired electron per metal center. Elemental analysis and mass spectrometry measurements were consistent with the proposed formulation for **6**.

A monocarbonyl complex, **7**, was prepared by the addition of 1 equiv of CO to a solution of **1** at −78 °C via Toepler line (Scheme 2). ^{1}H NMR spectroscopy showed that the reaction is quantitative, and red crystals of **7** were isolated from pentane at

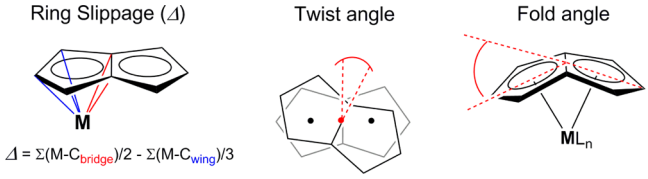

Figure 2. Definition of the ring slippage, twist angle, and fold angle parameters for pentalene structures.

Scheme 2. Reactivity of 1 with CO (R = $Si^{i}Pr_3$)

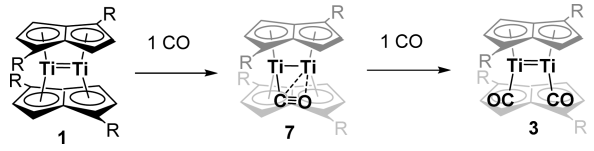

−35 °C in 62% yield. The solid-state structure of **7** (Figure 3) shows the CO ligand bound "side-on", asymmetrically bridging

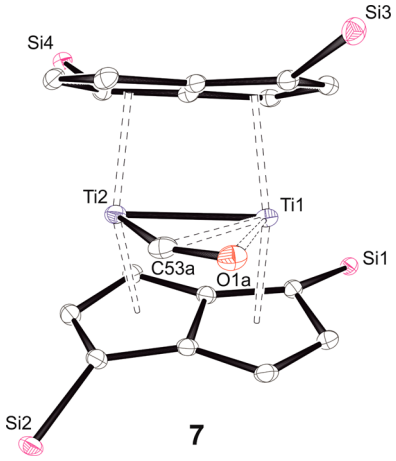

Figure 3. Displacement ellipsoid plot (30% probability) of **7** with hydrogen atoms and ^{i}Pr groups omitted for clarity.

the two Ti centers. The proximal Ti atom lies closer to the CO ligand in **7** than in the dicarbonyl complex **3**, and an additional interaction between the CO and the distal Ti atom is clearly in effect in the former complex (Ti1−C53a = 2.245(10) Å, Ti1−O1a = 2.294(5) Å), causing the O−C53−$Ti_{proximal}$ angle to deviate considerably from linearity (Table 1).

The ^{1}H NMR spectrum of **7** features eight doublet resonances in the aromatic region (see Figure S3 in the

Table 1. Selected Distances (Å), Angles (deg), and Values of the Parameters Defined in Figure 2 for 5, 7, 8, 11, and 12 (Ct Denotes the η^5 Centroid of a Pn Ring)

parameter	5	7	8	11	12
Ti−Ti	2.3991(7)	2.4047(5)	2.4432(10)	2.4880(8)	3.1402(6)
Ti−Ct[a]	2.133(10)	2.058(9)	2.104(13)	2.1088(13)	1.9470(18)
Ct−Ti−Ct[a]	139.722(12)	146.41(5)	138.02(9)	137.11(5)	57.09(9)
C53−$Ti_{proximal}$[a]	–	1.975(9)	2.238(4)	–	–
Ti−O/S[a]	1.8607(15)	2.352(6)	2.497(16)	2.3728(8)	2.323(2)
C53−O/S[a]	–	1.211(11)	1.657(4)	–	–
Δ[a]	0.150(19)	0.005(7)	0.114(4)	0.135(2)	–
twist angle	26.6(5)	20.1(8)	20.8(2)	20.3(2)	21.1(5)
fold angle[a]	0.15(13)	8.7(4)	4.6(2)	3.86(8)	17.30(12)

[a]Average values.

DOI: 10.1021/acs.organomet.5b00315
Organometallics 2015, 34, 4816−4829

Supporting Information), consistent with an unsymmetrical structure. The ^{1}H NMR spectrum of the isotopically labeled product [^{13}C]**7** differs from that of [^{12}C]**7** in that the Pn† ring signal at 7.69 ppm appears as a triplet (J = 3.2 Hz) with an ^{1}H−^{13}C (HMBC) correlation to the isotopically enriched μ-^{13}CO. Inspection of the ^{29}Si{^{1}H} NMR spectrum, which consists of four singlets for [^{12}C]**7**, reveals splitting of one signal into a doublet (J = 1.5 Hz) for [^{13}C]**7** (see Figure S4 in the Supporting Information). These features are attributed to through-space scalar couplings between the carbonyl carbon and the hydrogen and silicon in the proximal "wing-side" position of the Pn† ligands above and below the Ti_2CO plane (Figure 4). The average distance between the C_{CO} and these H

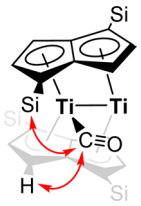

Figure 4. Through-space coupling between CO and Pn† wing-side substituents.

and Si atoms in the solid-state structure are 2.807(8) and 3.846(11) Å respectively. The solid-state IR spectrum of **7** exhibits a low ν(CO) stretching frequency of 1655 cm^{-1}, which shifts to 1616 cm^{-1} upon ^{13}C isotopic substitution, consistent with a side-on-bound carbonyl ligand.

Kinetic Studies. Experimentally, the reaction of **1** with CO_2 at low temperatures (between −90 and −30 °C) led to the quantitative formation of CO_2 adduct **4** (vide supra). When solutions of **4** were allowed to reach room temperature (in the absence of a dynamic vacuum) a color change from green to brown was observed, and the coordinated CO_2 molecule was reduced quantitatively over a period of minutes to give bis(oxo)-bridged dimer **2** and the dicarbonyl complex **3**. ^{1}H NMR spectra recorded during the course of this reaction showed additional transient species, including (as the major components) the mono(oxo) compound **5** and monocarbonyl complex **7**, identified by comparison with the spectra of independently synthesized samples.

The rate of decomposition of **4** was such that it could be conveniently followed by ^{1}H NMR spectroscopy. In a typical experiment, a 0.0295 M solution of **1** in MeCy-d_{14} at −78 °C (in the presence of ferrocene, with which **1** does not react, as an internal standard) was treated with 1 equiv of $^{13}CO_2$, and the resulting mixture was shaken over 30 min until complete conversion to dark-green **4** was observed. The reaction mixture was then placed in an NMR probe held at 20 °C and allowed to equilibrate thermally. The conversion of reactants to products was measured over time and showed first-order exponential decay of **4** (Figure 5). The rate constant for this process was therefore determined at seven different temperatures in the range 9−40 °C (see Table S3 in the Supporting Information), and the relevant Eyring plot is shown in Figure 6. The derived activation parameters are $\Delta H^{\ddagger}$ = 19.6 ± 1.0 kcal mol^{-1}, $\Delta S^{\ddagger}$ = −9 ± 3 e.u., and $\Delta G^{\ddagger}_{298\ K}$ = 22.4 ± 1.5 kcal mol^{-1}.

Reaction of CS_2 and COS with $Ti_2Pn^{\dagger}_2$. Heteroallenes CS_2 and COS are commonly used to model the reactivity of CO_2.[60,61] Treatment of a pentane solution of **1** with CS_2 at −35 °C gave a dark-green solution upon warming to room

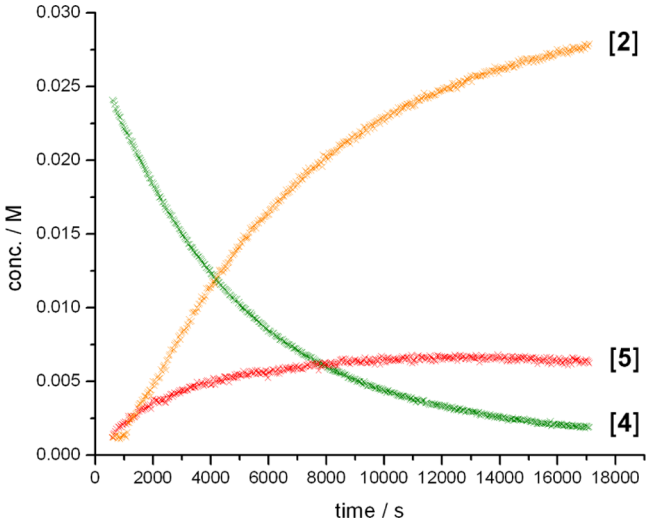

Figure 5. Concentration vs time curves for the decomposition of **4** to give oxo products **5** and **2** at 20 °C, as monitored by ^{1}H NMR spectroscopy.

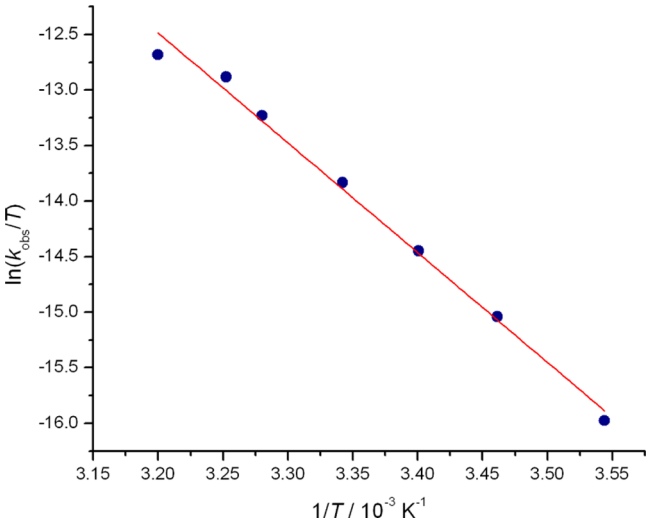

Figure 6. Eyring plot for the decomposition of **4** in MeCy-d_{14} (R^2 = 0.990).

temperature. Subsequent workup and cooling to −35 °C produced a red microcrystalline solid in 62% yield, which was identified by spectroscopic and analytical methods as **8** (Scheme 3). Crystals suitable for X-ray studies were grown

Scheme 3. Reaction of 1 with CS_2 (R = Si^{i}Pr$_3$)

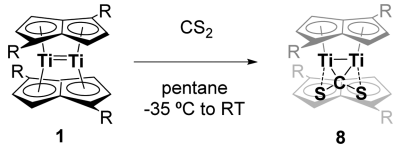

from an Et_2O solution, and the molecular structure (Figure 7) reveals a bent CS_2 molecule in a μ:η^2,η^2 binding mode between the two Ti centers.

The CS_2 ligand in **8** exhibits a S−C−S angle of 137.4(3)°, while the C−S bond lengths (av 1.657(4) Å) are longer than the C−S bond length in free CS_2 (1.554 Å).[62] The double-sandwich structure remains intact, with an elongated Ti−Ti

DOI: 10.1021/acs.organomet.5b00315
Organometallics 2015, 34, 4816−4829

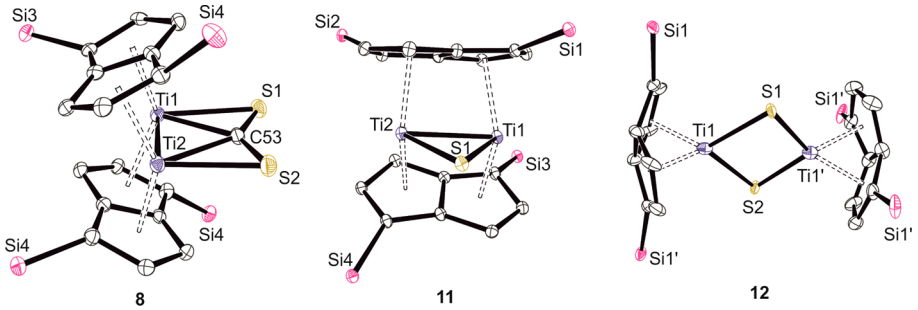

Figure 7. Displacement ellipsoid plots (30% probability) of **8**, **11**, and **12** with hydrogen atoms and ^{i}Pr groups omitted for clarity. Primed atoms are generated by symmetry.

distance (2.4432(10) Å) relative to **1** (2.399(2) Å)[54] and a smaller angle between the pentalene rings and the Ti_2 unit (av Ct−Ti−Ct = 138.02(9)°), giving a more open sandwich structure (Table 1). The ring slippage parameters (Figure 2) for each metal (Δ_{Ti1} = 0.145, 0.092; Δ_{Ti2} = 0.138, 0.082) indicate differential bonding to each side of the pentalene ligand.

The solid-state structure of **8** provides supporting evidence for the doubly bridging CO_2 ligand in **4**. However, **8** is stable at room temperature and does not decompose even upon heating to 100 °C, in stark contrast to the CO_2 adduct **4**, which decomposes above −30 °C to give the μ-oxo complex with concomitant liberation of carbon monoxide. This may be explained by the relative stability of CO compared with CS ($\Delta_f H^\circ_{298\ K}$ = −26.4 and 66.1 kcal mol^{-1}, respectively)[63,64] and the driving force for Ti−O bond formation ($\Delta_{bond}H^\circ_{298\ K}$ = 160.7 ± 2.2 kcal mol^{-1}) relative to Ti−S ($\Delta_{bond}H^\circ_{298\ K}$ = 99.9 ± 0.7 kcal mol^{-1}).[65] The notable difference in the reactivity of CS_2 versus CO_2 with **1** prompted a study with COS.

The reaction of **1** with 1 equiv of COS at −78 °C in MeCy-d_{14} produced a metastable adduct, **9**, that shows an ^{1}H NMR spectrum consistent with the loss of C_2 molecular symmetry, as opposed to those of the C_2-symmetric species **4** and **8**. The $^{13}C\{^1H\}$ NMR spectrum of **9** shows a singlet at 282 ppm, a value intermediate between those of the CO_2 and CS_2 analogues (219 and 356 ppm respectively). In situ IR spectroscopy at −65 °C showed a band at 1498 cm^{-1} which is tentatively assigned to the ν(CO) stretch of coordinated COS. However, the COS adduct **9** proved to be more thermally unstable than the CO_2 adduct **4**, and the coordinated molecule underwent scission to mono(μ-S) mono(CO) species **10** in 41% conversion as determined by ^{1}H NMR spectroscopy at −40 °C. Intermediate **10** was independently prepared by the reaction of mono(μ-S) complex **11** with 1 equiv of CO; **11** itself was readily synthesized by the reaction of **1** with Ph_3PS (Scheme 4) and fully characterized by spectroscopic and analytical methods (vide infra).

The synthesis of compound **11** was achieved by the reaction of **1** with 1 equiv of Ph_3PS in toluene (Scheme 4), and following workup **11** was isolated as red crystals in 52% yield. The proposed formulation of **11** is consistent with ^{1}H, ^{13}C, and ^{29}Si NMR and elemental analysis data and was ultimately confirmed by a single-crystal XRD study. The molecular structure of **11** (Figure 7) shows the sulfide ligand bridging the two Ti centers in a three-membered ring, akin to mono(μ-oxo) complex **5**. The Ti−Ti bond is considerably longer in **11** than in **5** (2.4880(8) and 2.3991(7) Å, respectively), and the larger bridging chalcogen atom is bonded at a greater distance from the Ti_2 core (av Ti−S = 2.3728(8); cf. av Ti−O = 1.8607(15)

Scheme 4. Reactivity of 1 with COS and Ph_3PS (R = Si^iPr_3)

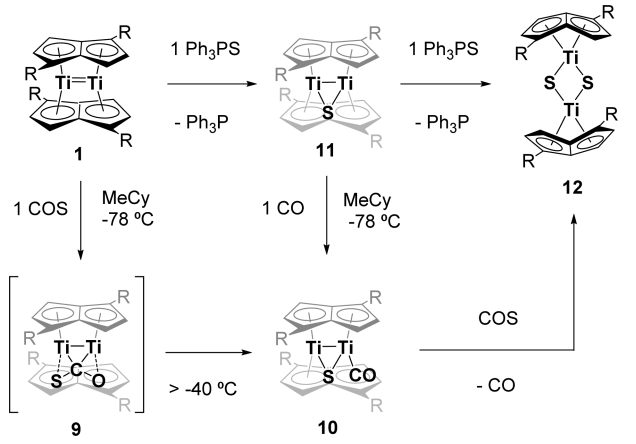

Å) with a more acute Ti−E−Ti angle (62.68(4)° and 80.28(8)°, respectively) (see Table 1). However, the smaller values of the Ti−Ct distance, ring slippage (Δ), and twist angle (Figure 2) for **11** reflect the fact that the Pn[†] ligands are more tightly bound compared with **5**, and this may explain the relative stability of this mono(μ-S) complex.

This triangular M−S−M structural motif is common among binuclear complexes with thiolato bridges but is unique in titanocene monosulfide chemistry. For example, $[Cp^*_2Ti]_2(\mu$-S) is a green paramagnetic complex with a Ti···Ti separation of 4.7069(7) Å and a Ti−S−Ti angle of 174.37(4)°.[66] The lack of a bonding (or an antiferromagentic coupling) interaction between the two d^1 centers in $[Cp^*_2Ti]_2(\mu$-S) gives rise to an electronic triplet state. In contrast, both **11** and **10** are diamagnetic.

The bis(μ-sulfide) complex **12** was independently synthesized by the reaction of **1** with 2 equiv of Ph_3PS in toluene (Scheme 4) and isolated in 80% yield. NMR spectroscopy, mass spectrometry, and elemental analysis confirmed the identity and purity of the product. Single crystals suitable for XRD analysis were grown from a saturated Et_2O solution at −35 °C, and its molecular structure is depicted in Figure 7, with important structural parameters listed in Table 1. Complex **12** is highly symmetrical; the solid-state structure shows a Ti_2S_2 unit that makes a regular ring with a perfectly planar diamond core (Ti1−S1−Ti1′−S1′ torsion angle = 0°). However, there is significant asymmetry in the Ti−S bond lengths (2.2238(16) and 2.4227(16) Å). The Ti−S−Ti angle is relatively acute (84.92(6)°), yet the Ti···Ti distance is considerably longer than in the bis(μ-oxo) congener (2.7376(6) Å).[55] The relative

DOI: 10.1021/acs.organomet.5b00315
Organometallics 2015, 34, 4816−4829

Table 2. Selected Calculated Structural Parameters (Å, deg) for Optimized Structures[a]

structure	Ti−Ti	Ti−Ct	Ct−Ti−Ct	Ti−C	Ti−O/S	C−O/S	Ti−O/S−Ti
Ti_2Pn_2 (**I**)[54]	2.37, *2.31*	2.00, *2.03*	153, *158*	–		–	–
$PnTiO_2TiPn$ (**II**)	2.74, *2.75*	2.00, *2.02*	56, *56*	–	1.87, *1.85*	–	95, *96*
$Ti_2Pn_2(CO)_2$ (**III**)	2.42, *2.42*	2.05, *2.05*	144, *144*	2.08, *2.08*		1.17, *1.17*	–
			142, *144*			1.17, *1.18*	
$Ti_2Pn_2CO_2$ (**IV**)	2.41, *2.40*	2.07, *2.10*	141, *141*	2.18, *2.14*	2.27, *2.25*	1.26, *1.29*	–
Ti_2Pn_2O (**V**)	2.38, *2.36*	2.13, *2.14*	139, *140*	–	1.87, *1.85*	–	79, *79*
PnTiOTiPn (*S* = 1) (**VIt**)	3.40, *3.69*	1.96, *1.99*	57, *57*	–	1.86, *1.85*	–	133, *180*
PnTiOTiPn (*S* = 0) (**VIs**)	2.88, *2.80*	1.96, *1.99*	57, *57*	–	1.85, *1.83*	–	103, *100*
Ti_2Pn_2CO (**VII**)	2.38, *2.36*	2.06, *2.08*	143, *143*	2.04, *2.02*	2.35, *2.26*	1.21, *1.25*	–
$Ti_2Pn_2CS_2$ (**VIII**)	2.43, *2.41*	2.10, *2.11*	138, *138*	2.27. *2.24*	2.54, *2.58*	1.67, *1.72*	–
Ti_2Pn_2COS (**IX**)	2.41, *2.40*	2.09, *2.11* (S)	138, *140* (S)	2.25, *2.20* (S)	2.63, *2.69* (S)	1.68, *1.73* (S)	–
		2.08, *2.09* (O)	140, *141* (O)	2.19, *2.17* (O)	2.19, *2.15* (O)	1.26, *1.29* (O)	
$Ti_2Pn_2S(CO)$ (**X**)	2.48, *2.47*	2.12, *2.13*	135, *136*	2.08, *2.07*	2.30, *2.31*	1.16, *1.18*	61, *61*
		2.11, *2.13*	136, *136*		2.54, *2.57*		
Ti_2Pn_2S (**XI**)	2.44, *2.42*	2.11, *2.12*	137, *140*	–	2.37, *2.39*	–	62, *61*
$PnTiS_2TiPn$ (**XII**)	3.13, *3.19*	1.98, *1.99*	*57*, *57*	–	2.33, *2.33*	–	84, *86*
$Ti_2Pn_2O(CO)$ (**Int1**)	2.46, *2.43*	2.18, *2.17*	135, *137*	2.08, *2.07*	1.76, *1.74*	1.16, *1.17*	–
		2.11, *2.13*	138, *138*		2.10, *2.07*		
Ti_2Pn_2OCO (**TS1**)	2.51, *2.50*	2.11, *2.13*	136, *136*	2.16, *2.14*	1.96, *1.93*	1.36, *1.40*	–
		2.09, *2.10*	143, *142*	2.75, *2.63*	3.16, *3.09*	1.23, *1.25*	

[a]ADF (BP/TZP) values are given in normal text, and Gaussian (B3LYP/SDD) values are given in *italics*.

orientation of the η^8-pentalene ligands (as defined by the angles between the two bridgehead C−C vectors) is 21.1(5)°.

Calculated Structures. Theoretical calculations were carried out on model systems with Pn (C_8H_6) as the ligand, mostly using two different functional/basis set combinations as embedded in two codes (ADF, BP/TZP; Gaussian, B3LYP/SDD). Selected calculated structural parameters are listed in Table 2 (in this article, experimentally observed/isolated compounds are labeled with Arabic numerals and their computational equivalents with the corresponding Roman numerals). In addition to the characterized compounds reported herein, structures were optimized for a possible intermediate and transition state in the transformation of **IV**.

DISCUSSION

Structure of $Ti_2Pn^{\dagger}{}_2CO_2$. Geometry optimization of the model system $Ti_2Pn_2CO_2$ (replacement of the silyl groups by H enhances the molecular symmetry) gave structure **IV** with C_{2v} symmetry and showing a bent CO_2 group bound symmetrically to the two Ti atoms (Figure 8). The calculated asymmetric and

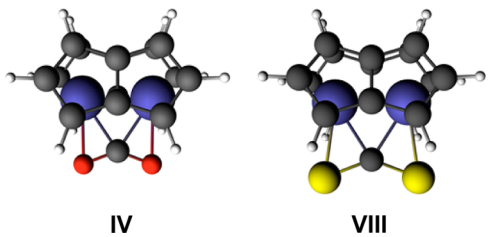

IV **VIII**

Figure 8. Optimized geometries of **IV** and **VIII**.

symmetric stretching modes for the CO_2 group are 1669 and 1214 cm^{-1}, respectively, which are in good agreement with the experimental results. Thus, we conclude that the high-symmetry NMR spectrum is a result of a symmetrical structure rather than a fast exchange process.

Carbon dioxide has been observed to bind to dinuclear metal sites with three different bonding modes (Figure 9).[10,67−69]

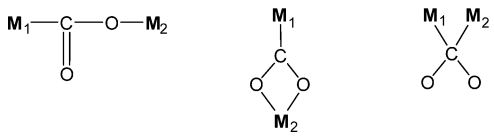

Figure 9. Crystallographically characterized bonding modes of CO_2 in bimetallic complexes.

The proposed μ:η^2,η^2- coordination geometry has only recently been structurally authenticated by X-ray crystallography in an N-heterocyclic carbene nickel(0) dimer, $[(IPr)Ni]_2(\mu$-CO)-(μ:η^2,η^2-CO_2) (IPr = 1,3-bis(2,6-diisopropylphenyl)imidazol-2-ylidene).[70]

Support for the symmetrical binding of CO_2 is provided by the authenticated structure of the sulfur analogue. Geometry optimization of $Ti_2Pn_2CS_2$ also resulted in a structure **VIII** of C_{2v} symmetry (Figure 8), in good agreement with the experimental stucture of **8.** The solution IR spectrum of **8** shows a band at 1104 cm^{-1} which, compared with the asymmetric stretch of free CS_2 (1535 cm^{-1}),[71] is consistent with a sulfur-bound CS_2 moiety. This is in fair agreement with the stretching vibration for the model system **VIII** (1079 cm^{-1}) calculated by DFT methods.[56] Precedent for this type of CS_2 coordination involving both C═S π bonds is limited to a single example of a dinuclear Cu(I) complex recently reported by Limberg and co-workers.[72] However, in this complex the mean plane of the CS_2 atoms is twisted with respect to the M−C−M mean plane by 49.1°, whereas in **8** these planes are nearly parallel (3.1°).

Structure of $Ti_2Pn^{\dagger}{}_2CO$. The side-on binding of CO in **7** is sufficiently unusual to deserve comment. Compound **7** is, to the best of our knowledge, the first example of a "semibridging" carbonyl ligand between two titanium centers, and hetero-metallic examples involving titanium carbonyls are very rare. A weak semibridging carbonyl−gold interaction was inferred in

DOI: 10.1021/acs.organomet.5b00315
Organometallics 2015, 34, 4816−4829

the anionic gold−titanium complex $[K(15\text{-crown-}5)_2][Ti(CO)_6(AuPEt_3)]$ on the basis of X-ray structural parameters and a difference between the solid-state and solution IR ν(CO) stretching frequencies.[73] Semibridging carbonyls have also been observed in the aforementioned Ti/M heterobimetallics $Cp_2Ti(\mu\text{-}PEt_3)(\mu\text{-}\eta^1{:}\eta^2\text{-}OC)M(CO)Cp$ (M = Mo, W),[74] $Cp_2Ti(\mu\text{-}C\{R\}CH_2)(\mu\text{-}\eta^1{:}\eta^2\text{-}OC)W(CO)Cp$,[75,76] and $Cp_2Ti(\mu\text{-}CR)(\mu\text{-}\eta^1{:}\eta^2\text{-}OC)W(CO)Cp$ (R = *p*-Tol),[77] which show substantial reduction in the C−O bond order compared with typical terminal carbonyl moieties, as evidenced by the C−O bond distance and ν(CO).

The geometric function $\Omega = \exp[d(M_{distal}\text{−}C)/d(M_{distal}\text{−}O)]$ measures the extent of the interactions of the distal metal atom with the C and O ends of the CO ligand.[78] This function can be used to differentiate between C- and O-bonded metal carbonyls in "end-on" (Σ-CO) and "side-on" (Π-CO) disposition. The average value for **7** (Ω = 2.69) lies comfortably in the range for a Π-CO (typically 2.2 < Ω < 3.3), and comparable values have been found for Ti/M heterobimetallics with semibridging CO ligands: $Cp_2Ti(\mu\text{-}C\{p\text{-}Tol\}CH_2)(\mu\text{-}\eta^1{:}\eta^2\text{-}OC)W(CO)Cp$ (Ω = 2.65)[75,76] and $Cp_2Ti(\mu\text{-}C\{p\text{-}Tol\})(\mu\text{-}\eta^1{:}\eta^2\text{-}OC)W(CO)Cp$ (Ω = 2.63).[77] The C−O bond distance in **7** (av 1.211(11) Å) is lengthened with respect to that in free CO (1.128 Å)[79] to an extent that is comparable to the Σ-CO complexes $Cp_2Ti(THF)(\mu\text{-}OC)Mo(CO)_2Cp$ (1.201(8) Å)[80] and $Cp^*_2Ti(Me)(\mu\text{-}OC)Mo(CO)_2Cp$ (1.212(5) Å),[81] in which the titanocene moiety behaves as a Lewis acid, coordinating to an oxygen atom of the Lewis basic $[CpMo(CO)_3]^-$ fragment.

Geometry optimization of Ti_2Pn_2CO resulted in a structure with C_s symmetry (**VII**) in which the carbonyl ligand is bound side-on to the Ti dimer (Figure 10). A double bond is retained between the two Ti atoms in **VII**,[56] and the calculated Ti−Ti distance (2.38, *2.36* Å) is in reasonable agreement with the X-ray data (2.4047(5) Å). The wavenumber for the CO stretch in **VII** was calculated as 1644 cm^{-1}, which is in the low end of the range for symmetric bridging carbonyls (1850−1600 cm^{-1})[82] but in good agreement with the experimental value of 1655 cm^{-1} in **7**. The disfavoring of a symmetrically bridged CO is attributable to the absence of a high-lying orbital of suitable symmetry for back-donation in **1**.[56]

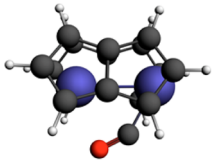

Figure 10. Optimized geometry of **VII**.

Thermal Transformations of $Ti_2Pn^{\dagger}_2CO_2$. The fate of **4** upon warming depends on whether the solution is sealed or under dynamic vacuum. Removing CO from the reaction leads to the formation of **5**, which undergoes further reaction to give its isomer **6**. A possible intermediate, undetected as yet experimentally, in the decomposition of $Ti_2Pn^{\dagger}_2CO_2$ (**4**) is $Ti_2Pn^{\dagger}_2(\mu\text{-}O)CO$, in which a CO bond has broken, the detached O bridges the two Ti atoms, and the CO ligand formed is bonded to one of the Ti atoms. Geometry optimization of $Ti_2Pn_2(\mu\text{-}O)CO$ gave a local minimum for such a species, **Int1** (Figure 11), in which the Ti−Ti distance (2.46, *2.43* Å) is still indicative of metal−metal bonding. The bridging O is placed asymmetrically, further from the Ti to which the CO is coordinated. The search for a transition state between **IV** and **Int1** yielded structure **TS1** shown in Figure 11, with geometric parameters given in Table 2; the transition state also possesses C_s symmetry. Both a Ti−C and a Ti−O bond are breaking and the remaining Ti−O bond has shortened, but the new Ti−O bond to the bridging O has not yet formed.

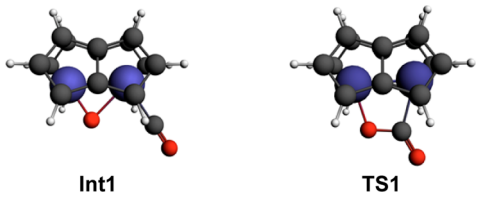

Figure 11. Optimized geometries of **Int1** and **TS1**.

Loss of CO from $Ti_2Pn_2O(CO)$ (**Int1**) leads to a mono(oxo) product. Maintenance of the double-sandwich structure of the Ti_2Pn_2 fragment leads to a local minimum with C_{2v} symmetry, structure **V**. Two other structures were found with η^8 coordination of Pn to Ti, one with a triplet state, **VIt**, and the other with a singlet state, **VIs** (Figure 12). The structures found for the triplet state by the two methods differed in the Ti−O−Ti angle: the ADF (BP/TZP) calculations optimized to a bent angle, while the Gaussian (B3LYP/SDD) calculations gave a linear Ti−O−Ti unit. Similar structures with η^8 coordination were found for the singlet state by the two methods (Table 2). The energies of all three structures are close, and which structure is the most stable is method- and temperature-dependent (Table 3): ADF (BP/TZP) has the double-sandwich structure as the most stable, while Gaussian (B3LYP/SDD) estimates the SCF energy of the sandwich structure to be the lowest but on the basis of the free energy at 298 K predicts the triplet η^8-coordinated structure to

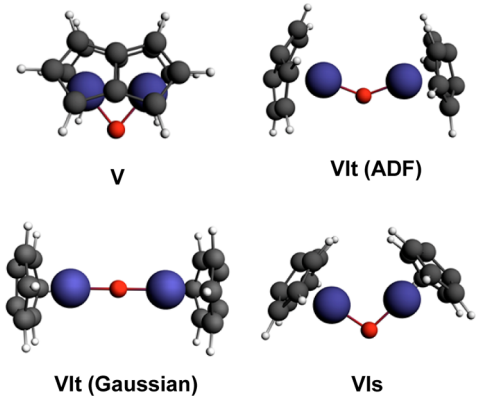

Figure 12. Optimized geometries of the mono(oxo) species **V**, **VIt**, and **VIs**.

Table 3. Ti−O−Ti Angles (deg) and Relative Energies (kcal mol^{-1}) of Structures Found for Ti_2Pn_2O[56,a]

structure	Ti−O−Ti	ΔE(SCF)	$\Delta H^{\circ}_{298\ K}$	$\Delta G^{\circ}_{298\ K}$
V	79, *79*	0, *0*	0, *0*	0, *2*
VIt	133, *180*	12, *4*	13, *3*	8, *0*
VIs	103, *100*	12, *19*	13, *21*	10, *20*

[a]ADF (BP/TZP) values are given in normal text, and Gaussian (B3LYP/SDD) values are given in *italics*.

DOI: 10.1021/acs.organomet.5b00315
Organometallics 2015, 34, 4816−4829

be the most stable. This is in agreement with experiment, as the double-sandwich structure **5** is known to convert to the triplet state **6** at room temperature. The large ring slippage and twist angle found in the solid-state structure of **5** may be construed as a "snapshot" of the Pn† rings as they move across the Ti_2 core from a bridging (μ-η^5,η^5) bonding mode in **5** toward a capping (η^8) mode in the structural isomer **6**.

The free energy profile found for the binding of CO_2 to **I** and the transformation of **IV** when CO is removed is given in Figure 13 (the reaction pathway of **V** to form **VIt** was too

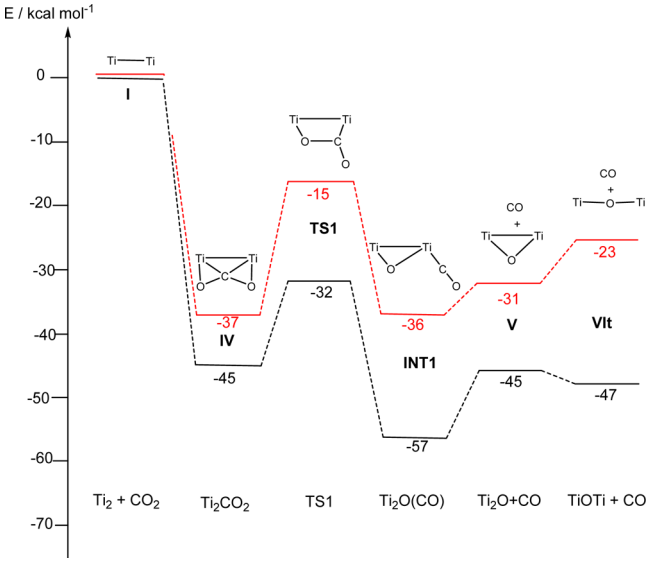

Figure 13. Free energies for binding of CO_2 to **I** and the decomposition of **IV** under dynamic vacuum. ADF (BP/TZP) values are given in red and Gaussian (B3LYP/SDD) values in black.

complex to model). Binding of CO_2 to **I** is strongly favored, but the activation energy calculated for the decomposition of **IV** (22, *13* kcal mol^{-1}) is reasonably accessible at room temperature.

The decomposition of **4** to **6** via **5** when CO is removed and the detection of **5** when CO is present strongly suggest that a similar route is followed when the decomposition proceeds further in the presence of CO (see Scheme 1). DFT calculations were used to examine the possible pathways for the formation of **2** and **3** (eqs 1−5 below; in the chemical formulas, the Pn ligands have been omitted; numbers in Roman numerals refer to the optimized, calculated structures in Table 2; numbers at the right are ADF, *Gaussian* reaction free energies).

$$Ti_2O(\mathbf{V}) + TiOTi(\mathbf{VIt}) \rightarrow Ti_2(\mathbf{I}) + TiO_2Ti(\mathbf{II})$$
$$-8,\ \mathit{0}\ \text{kcal mol}^{-1} \quad (1)$$

$$Ti_2O(CO)(\mathbf{Int1}) + TiOTi(\mathbf{VIt}) \rightarrow Ti_2CO(\mathbf{VII}) + TiO_2Ti(\mathbf{II}) \quad -33,\ -\mathit{22}\ \text{kcal mol}^{-1} \quad (2)$$

$$Ti_2(\mathbf{I}) + CO \rightarrow Ti_2CO(\mathbf{VII}) \quad -31,\ -33\ \text{kcal mol}^{-1} \quad (3)$$

$$Ti_2CO(\mathbf{VII}) + CO \rightarrow Ti_2(CO)_2(\mathbf{III})$$
$$-12,\ -\mathit{23}\ \text{kcal mol}^{-1} \quad (4)$$

$$2Ti_2CO_2(\mathbf{IV}) \rightarrow Ti_2(CO)_2(\mathbf{III}) + TiO_2Ti(\mathbf{II})$$
$$-30,\ -\mathit{60}\ \text{kcal mol}^{-1} \quad (5)$$

Consideration of eqs 1 and 2 suggests that **VI** is oxophilic and attacks either **V** or the proposed oxocarbonyl intermediate (**Int1**) to form the bis(oxo) complex **II**. The more favorable values found for the reaction shown in eq 2 indicate that the

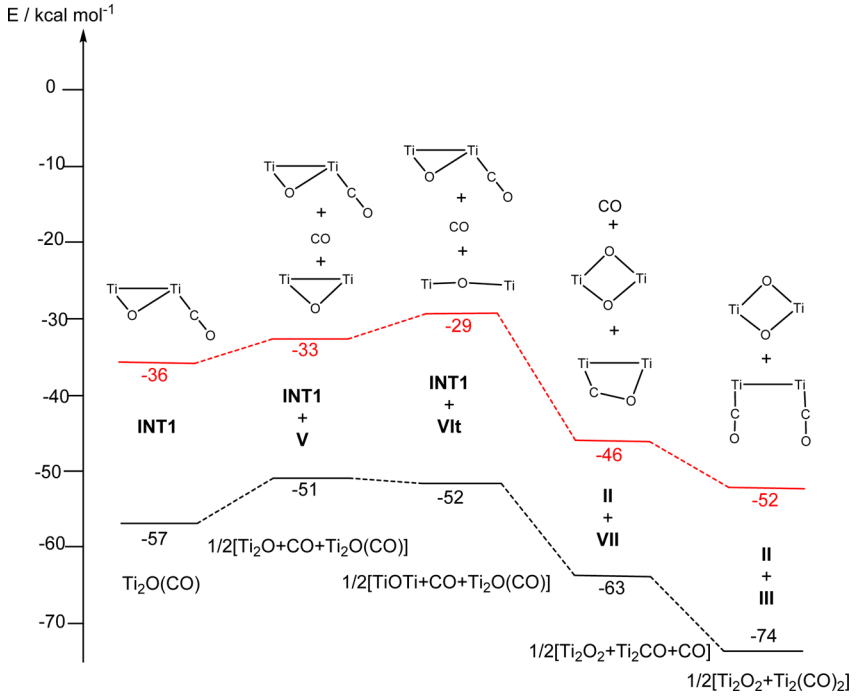

Figure 14. Calculated free energies of intermediates in the disproportionation of $Ti_2Pn_2O(CO)$ (**Int1**). Zero represents the energy of $Ti_2Pn_2CO_2$ (**IV**). ADF (BP/TZP) values are shown in red and Gaussian (B3LYP/SDD) values in black.

DOI: 10.1021/acs.organomet.5b00315
Organometallics 2015, 34, 4816−4829

presence of CO helps drive the disproportionation, explaining the lack of further decomposition when CO is removed from the reaction. Binding of a further molecule of CO to form the dicarbonyl **III** (eq 4) is favorable but not as exothermic as forming the monocarbonyl (eq 3). The overall decomposition is found to be thermodynamically favorable (eq 5). That the reaction appears to be first order suggests that the rate-determining step is the initial rupture of the bound CO_2 to form the proposed intermediate, rather than any subsequent disproportionation process, which would result in a second-order or more complex rate expression. Figure 14 shows the energies of intermediates involved in a possible disproportionation route. The experimental activation energy ($\Delta G^{\ddagger}_{298\ K}$ = 22.4 ± 1.5 kcal mol^{-1}) is in good agreement with the ADF (BP/TZP)-calculated activation energy for the decomposition of **IV** (22 kcal mol^{-1}; vide supra).

In terms of the final products of the reaction of **I** with CO_2, geometry optimization of $Ti_2Pn_2(CO)_2$ (**III**) by both ADF (BP/TZP) and Gaussian (B3LYP/SDD) gave a structure of C_s symmetry only slightly displaced from C_{2v} symmetry (Figure 15), which agrees well with that found experimentally. The

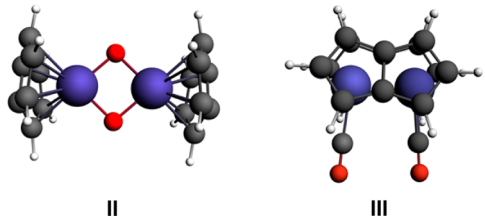

Figure 15. Optimized geometries of **II** and **III**.

calculated wavenumbers for the antisymmetric and symmetric CO stretches in **III** are 1947, *1899* cm^{-1} and 1878, *1810* cm^{-1}, respectively, which are higher than the ν(CO) values found experimentally in **3** (1910 and 1987 cm^{-1}). The optimized structure of **II** had C_{2h} symmetry (Figure 15) with eclipsed pentalene rings and the Ti_2O_2 plane at an angle of 22° with respect to the pentalene bridging carbons.

Preliminary trials on an NMR scale to observe the proposed mono(μ-oxo) mono(CO) intermediate by reaction of [^{13}C]**7** with 1 equiv of N_2O or **5** with 1 equiv of ^{13}CO were inconclusive. The ^{13}C{^{1}H} NMR spectra were complex in each case, with the dicarbonyl complex [^{13}C]**3** identified as the major labeled product after warming to room temperature. ^{1}H NMR spectra confirmed the presence of bis(oxo) **2** in each case, which is a thermodynamic sink in the reaction of **1** with CO_2 because of the formation of strong Ti−O bonds.

Reaction of COS with $Ti_2Pn^{\dagger}_2$. Support for the proposed intermediate comes from the reaction sequence observed when COS is added to **1**. The first formed species, **9**, shows a CO stretch at 1498 cm^{-1}, which is in good agreement with the stretching vibration at 1487 cm^{-1} for model system **IX** (Figure 16) calculated by DFT methods.[56]

The free energy of the reaction of **I** with COS is intermediate between that of CS_2 (−52 kcal mol^{-1}) and CO_2 (−37 kcal mol^{-1}) (eq 6).

$$Ti_2(\mathbf{I}) + COS \rightarrow Ti_2COS(\mathbf{IX}) \quad -44,\ -47\ \text{kcal mol}^{-1} \tag{6}$$

The formation of **X**, from **IX**, is calculated to be slightly favorable (eq 7) with an activation energy of 32, *21* kcal mol^{-1}. The value found for the equivalent reaction to **Int1** is 22, *13*

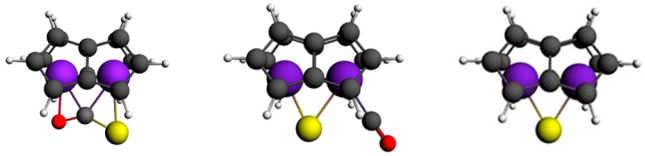

Figure 16. Optimized geometries of **IX**, **X**, and **XI**.

kcal mol^{-1}. Loss of CO from **X** is unfavorable (eq 8) and more so than from **Int1** (5, *11* kcal mol^{-1}).

$$Ti_2COS(\mathbf{IX}) \rightarrow Ti_2S(CO)(\mathbf{X}) \quad -3,\ -9\ \text{kcal mol}^{-1} \tag{7}$$

$$Ti_2S(CO)(\mathbf{X}) \rightarrow Ti_2S(\mathbf{XI}) + CO \quad +11,\ +17\ \text{kcal mol}^{-1} \tag{8}$$

The mono(μ-S) mono(CO) intermediate **10** was too unstable to be isolated in the solid state but was characterized by spectroscopic methods in solution. In situ IR spectroscopy showed a broad band at 2011 cm^{-1}, in the expected region for a terminal CO ligand, that shifted to 1966 cm^{-1} in the isotopically labeled [^{13}C]**11**. The calculated structure **X** (Figure 16) has a CO vibration at 1937 cm^{-1}. The discrepancy here is rather large. The ^{1}H NMR spectrum of **10** consists of four doublets in the aromatic region, indicative of chemically equivalent $Pn^{\dagger}$ rings on the NMR time scale. This can be attributed to a fluxional process involving intramolecular exchange of CO between the two Ti centers that results in an averaged NMR structure of C_2 symmetry.

In the presence of excess of COS, green solutions of **10** decompose within hours at room temperature to give a brown solution (Scheme 4). ^{1}H NMR spectroscopy of the brown solution showed near-quantitative conversion to the bis(μ-S)-bridged dimer [(η^8-$Pn^{\dagger}$)Ti(μ-S)]$_2$ (**12**) as the sole Ti-containing product, in contrast to the decomposition of CO_2 adduct **4**, which also gives dicarbonyl complex **3**. The related oxo species, $Ti_2Pn_2O(CO)$ (**Int1**), was implicated in the DFT-modeled pathway of the CO_2 reaction but was not observed experimentally.

The free energy of formation of **VIII** is calculated as −53 kcal mol^{-1}, which is significantly greater than that of **IV**. The energy to form equivalent decomposition products is unfavorable (eq 9), and we were unable to identify computationally an intermediate equivalent to **Int1** where a C−S bond had been ruptured and bound CS formed; instead, the structure reverted to an alternative η^2 mode of CS binding.

$$2Ti_2CS_2(\mathbf{VIII}) \rightarrow Ti_2(CS)_2 + TiS_2Ti(\mathbf{XIII}) \quad +15\ \text{kcal mol}^{-1} \tag{9}$$

CONCLUSIONS

Complex **1** shows unique reactivity among bis(pentalene)-dimetal double-sandwich complexes, including multiple adduct formation with carbon monoxide and reductive activation of carbon dioxide. Mechanistic studies show that **1** binds CO_2 at low temperatures, but this adduct **4** is thermally unstable and upon warming to room temperature, reaction of the coordinated CO_2 molecule occurs. We have gained significant insight into the mechanism for this reaction using synthetic, spectroscopic, and computational methods to identify key intermediates. Thermally driven cleavage of the bound CO_2 occurs to give oxo and carbonyl fragments, and exposure of **4** to

DOI: 10.1021/acs.organomet.5b00315
Organometallics 2015, 34, 4816−4829

dynamic vacuum removes CO, allowing the isolation of a diamagnetic mono(oxo) complex, **5**. The latter shows a strained three-membered "dimetallaepoxide" motif in its molecular structure and is unstable at room temperature with respect to the paramagnetic, bridging mono(oxo) complex **6**, in which the Ti^{III} centers are better stabilized, electronically and sterically, with η^8-bound pentalene ligands.

The reactivity of **1** with the heteroallenes CS_2 and COS provides useful insight in comparison with that observed for CO_2. The thermally stable CS_2 adduct **8** shows symmetrical binding to the Ti_2 unit, providing supporting evidence for the doubly bridging CO_2 ligand in **4**. **1** displays greater, and different, reactivity toward COS, but some parallels can be made with the CO_2 reaction. The asymmetric COS molecule undergoes scission at low temperatures, forming the mono(μ-S) mono(CO) species **10**, which has sufficient stability for spectroscopic characterization. A mono(μ-O) mono(CO) counterpart was implicated in the CO_2 reaction pathway but was not observed experimentally.

EXPERIMENTAL SECTION

General Procedures. All manipulations were carried out using standard Schlenk techniques under Ar or in an MBraun glovebox under N_2 or Ar. All glassware was dried at 160 °C overnight prior to use. Solvents were purified by predrying over sodium wire and then distilled over Na (toluene), K (methylcyclohexane), or Na–K alloy (Et_2O and pentane) under a N_2 atmosphere. Dried solvents were collected, degassed, and stored over argon in K-mirrored ampules. Deuterated solvents were degassed by three freeze–pump–thaw cycles, dried by refluxing over K for 3 days, vacuum-distilled into ampules, and stored under N_2. The gases used were of very high purity—CO (99.999%) and CO_2 (99.99%) were supplied by Union Carbide, COS (>97.5%) was supplied by Aldrich, N_2O (purity >99.998%) was supplied by Fluka—and all gases were added via Toepler line. Isotopically enriched gases, ^{13}CO (99.7%) and $^{13}CO_2$ (99%), were supplied by Euriso-top and Cambridge Isotopes, respectively, and added via Toepler pump. Triphenylphosphine sulfide (98%) was purchased from Aldrich and used as received. The compounds $Ti_2Pn^{\dagger}_2$ (**1**),[54] $Ti_2Pn^{\dagger}_2O_2$ (**2**), and $Ti_2Pn^{\dagger}_2(CO)_2$ (**3**)[55] were prepared according to published procedures. NMR spectra were recorded on a Varian VNMRS 400 spectrometer (^1H, 399.5 MHz; $^{13}C\{^1H\}$, 100.25 MHz; $^{29}Si\{^1H\}$, 79.4 MHz). The ^1H and ^{13}C spectra were referenced internally to the residual protic solvent (^1H) or the signals of the solvent (^{13}C). $^{29}Si\{^1H\}$ NMR spectra were referenced externally relative to $SiMe_4$. IR spectra were recorded between NaCl plates using a PerkinElmer Spectrum One FTIR instrument or a Mettler-Toledo ReactIR system featuring an IR probe inside a gas-tight cell attached to a Toepler pump. Mass spectra were recorded using a VG Autospec Fisons instrument (EI at 70 eV). Elemental analyses for were carried out at the Elemental Analysis Service, London Metropolitan University.

Syntheses. *$Ti_2(\mu{:}\eta^5,\eta^5\text{-}Pn^{\dagger})_2CO_2$ (4).* A J. Young NMR tube was charged with **1** (16 mg, 0.017 mmol) and methylcyclohexane-d_{14} (0.5 mL), and the solution was cooled to −78 °C. The headspace was evacuated, and CO_2 (0.017 mmol) was admitted. The tube was briefly shaken, and a color change from deep red to dark green was observed. NMR spectra were immediately measured, with the probe precooled to −30 °C. Alternatively, using $^{13}CO_2$ in the method above yielded the labeled product [^{13}C]**4**. NMR yield: quantitative with respect to **1**. ^1H NMR (methylcyclohexane-d_{14}, 399.5 MHz, 243 K): δ_H 5.98 (2H, d, $^3J_{HH}$ = 3.6 Hz, Pn *H*), 5.83 (2H, d, $^3J_{HH}$ = 2.9 Hz, Pn *H*), 5.66 (2H, d, $^3J_{HH}$ = 2.8 Hz, Pn *H*), 5.37 (2H, d, $^3J_{HH}$ = 3.6 Hz, Pn *H*), 0.69 (6H, dt, $^3J_{HH}$ = 7.4, 14.9 Hz, ^{i}Pr C*H*), 0.57 (6H, dt, $^3J_{HH}$ = 7.4, 14.7 Hz, ^{i}Pr C*H*), 0.34 (18H, d, $^3J_{HH}$ = 7.3 Hz, ^{i}Pr CH_3), 0.31 (18H, d, $^3J_{HH}$ = 7.5 Hz, ^{i}Pr CH_3), 0.20 (18H, d, $^3J_{HH}$ = 7.4 Hz, ^{i}Pr CH_3), 0.16 (18H, d, $^3J_{HH}$ = 7.4 Hz, ^{i}Pr CH_3). $^{13}C\{^1H\}$ NMR (methylcyclohexane-d_{14}, 100.5 MHz, 243 K, selected data): δ_C 219 (s, CO_2). $^{29}Si\{^1H\}$ NMR (methylcyclohexane-d_{14}, 79.4 MHz, 243 K): δ_{Si} 2.12, 1.88. IR (methylcyclohexane, −65 °C): **4** 1678 (ν_{asym}(OCO)), 1236 (ν_{sym}(OCO)) cm^{-1}; [^{13}C]**4** 1637 (ν_{asym}(O^{13}CO)), 1217 (ν_{sym}(O^{13}CO)) cm^{-1}. EI-MS and microanalysis data were not obtained for **4** because of its susceptibility to further reaction above 0 °C.

$Ti_2(\mu{:}\eta^5,\eta^5\text{-}Pn^{\dagger})_2(\mu\text{-}O)$ (5). Method A: A J. Young NMR tube was charged with **1** (17 mg, 0.018 mmol) and C_6D_6 (0.6 mL), and the solution was frozen at −78 °C. The headspace was evacuated, and N_2O (0.016 mmol) was admitted. The tube was warmed to room temperature, and a color change to bright red was observed as the solution thawed. NMR yield: 68% with respect to **1**. Method B: An ampule charged with **1** (78.5 mg, 0.0848 mmol) and methylcyclohexane (5 mL) was cooled to −78 °C, and the headspace was evacuated. CO_2 gas (1 atm) was admitted, resulting in a color change from deep red to dark green. The ampule was placed under reduced pressure and then removed from the −78 °C bath. The solvent was slowly removed in vacuo as the reaction mixture warmed to room temperature, giving a crude red residue. Recrystallization from toluene (1 mL) at −35 °C afforded **5** as a red microcrystalline solid. Total yield: 66.3 mg (83% with respect to **1**). Subsequent recrystallization from a concentrated toluene/pentane solution at −35 °C afforded X-ray-quality crystals. ^1H NMR (C_6D_6, 399.5 MHz, 303 K, selected data): δ_H 7.86 (2H, d, $^3J_{HH}$ = 3.3 Hz, Pn *H*), 6.78 (2H, d, $^3J_{HH}$ = 3.2 Hz, Pn *H*), 6.45 (2H, d, $^3J_{HH}$ = 3.2 Hz, Pn *H*), 6.39 (2H, d, $^3J_{HH}$ = 3.2 Hz, Pn *H*), 1.55 (6H, m, ^{i}Pr C*H*), 1.26 (6H, m, ^{i}Pr C*H*), 1.13 (18H, d, $^3J_{HH}$ = 7.2 Hz, ^{i}Pr CH_3), 1.10 (18H, d, $^3J_{HH}$ = 7.4 Hz, ^{i}Pr CH_3), 1.01 (18H, d, $^3J_{HH}$ = 7.4 Hz, ^{i}Pr CH_3), 0.96 (18H, d, $^3J_{HH}$ = 7.4 Hz, ^{i}Pr CH_3). $^{13}C\{^1H\}$ NMR (C_6D_6, 100.5 MHz, 303 K, selected data): δ_C 134.2 (Pn *C*), 133.4 (Pn *C*), 132.6 (Pn *C*), 114.9 (Pn *C*), 111.3 (Pn *C*), 108.1 (Pn *C*), 102.2 (Pn *C*), 99.47 (Pn *C*), 19.94 (^{i}Pr CH), 19.89 (^{i}Pr CH), 19.39 (^{i}Pr CH_3), 19.35 (^{i}Pr CH_3), 14.11 (^{i}Pr CH), 12.97 (^{i}Pr CH). $^{29}Si\{^1H\}$ NMR (C_6D_6, 303 K): δ_{Si} 2.39, 1.01. EI-MS: *m*/*z* 941 (100%) [M]$^+$. Anal. Found (Calcd for $C_{52}H_{92}OSi_4Ti_2$): C, 66.21 (66.35); H, 9.70 (9.85) %.

$[(\eta^8\text{-}Pn^{\dagger})Ti]_2(\mu\text{-}O)$ (6). Storage of a C_6D_6 solution of **5** (6.6 μmol) overnight at room temperature afforded green crystals of **6**, which were isolated by decantation, washed with cold pentane (1 mL, −35 °C) and dried in vacuo. Total yield: 2.0 mg (32% with respect to **5**). ^1H NMR (toluene-d_8, 399.5 MHz, 303 K): δ_H 4.09 (br, $\Delta\nu_{1/2}$ = 138 Hz, Pn *H*), 4.09 (br, $\Delta\nu_{1/2}$ = 138 Hz, Pn *H*), 1.77 (br, $\Delta\nu_{1/2}$ = 110 Hz, ^{i}Pr C*H*), 1.13 (br, $\Delta\nu_{1/2}$ = 106 Hz, ^{i}Pr CH_3). ^{13}C and ^{29}Si NMR resonances were not observed because of the paramagnetic nature of **6**. EI-MS: *m*/*z* 941 (100%) [M]$^+$. Anal. Found (Calcd for $C_{52}H_{92}OSi_4Ti_2$): C, 66.17 (66.35); H, 9.75 (9.85) %. Magnetic susceptibility (Evans method, THF-d_8, 303 K): μ_{eff} = 2.45μ_B per molecule = 1.73μ_B per Ti.

$Ti_2(\mu{:}\eta^5,\eta^5\text{-}Pn^{\dagger})_2(\mu{:}\eta^2\text{-}CO)$ (7). An ampule charged with **1** (50 mg, 0.054 mmol) and toluene (0.5 mL) was cooled to −78 °C, and the headspace was evacuated. CO gas (0.9 molar equiv, 0.050 mmol) was admitted slowly to the mixture with vigorous stirring, resulting in a color change from deep red to purple. After the mixture was warmed to room temperature, the volatiles were removed in vacuo to afford a crude purple solid that was recrystallized from pentane (1 mL) at −35 °C. Total yield: 32 mg (62% with respect to **1**). Alternatively, exposing a methylcyclohexane-d_{14} solution of **1** to 0.9 equiv of ^{13}CO via Toepler pump yielded the labeled product [^{13}C]**7**. ^1H NMR (methylcyclohexane-d_{14}, 399.5 MHz, 303 K): δ_H 7.69 (1H, apparent t, $^3J_{HH}$ = 3.2 Hz, Pn *H*), 7.10 (1H, d, $^3J_{HH}$ = 3.2 Hz, Pn *H*), 6.62 (1H, d, $^3J_{HH}$ = 3.5 Hz, Pn *H*), 6.34 (1H, d, $^3J_{HH}$ = 3.5 Hz, Pn *H*), 6.30 (2H, d, $^3J_{HH}$ = 3.2 Hz, Pn *H*), 6.22 (2H, d, $^3J_{HH}$ = 3.6 Hz, Pn *H*), 5.74 (1H, d, $^3J_{HH}$ = 3.5 Hz, Pn *H*), 5.62 (1H, d, $^3J_{HH}$ = 3.2 Hz, Pn *H*), 1.62–1.25 (12H, overlapping m, ^{i}Pr C*H*), 1.25–0.83 (72H, overlapping m, ^{i}Pr CH_3). $^{13}C\{^1H\}$ NMR (methylcyclohexane-d_{14}, 100.5 MHz, 303 K): δ_C 295.1 (s, CO), 136.8 (Pn *C*), 132.5 (Pn *C*), 132.4 (Pn *C*), 129.1 (Pn *C*), 127.7 (Pn *C*), 125.1 (Pn *C*), 124.9 (Pn *C*), 115.1 (Pn *C*), 108.2 (Pn *C*), 104.7 (Pn *C*), 103.2 (Pn *C*), 101.5 (Pn *C*), 99.75 (Pn *C*), 95.08 (Pn *C*), 93.16 (Pn *C*), 89.87 (Pn *C*), 20.94 (^{i}Pr CH_3), 20.84 (^{i}Pr CH_3), 20.79 (^{i}Pr CH_3), 20.64 (^{i}Pr CH_3), 20.62 (^{i}Pr CH_3), 20.37 (^{i}Pr CH_3), 20.36 (^{i}Pr CH_3), 20.13 (^{i}Pr CH_3), 15.14 (^{i}Pr CH), 15.12 (^{i}Pr CH), 14.45 (^{i}Pr CH), 14.22 (^{i}Pr CH). $^{29}Si\{^1H\}$ NMR (methylcyclohexane-

DOI: 10.1021/acs.organomet.5b00315
Organometallics 2015, 34, 4816–4829

d_{14}, 79.4 MHz, 303 K): δ_{Si} 3.40 (s), 2.88 (d, J_{SiC} = 1.2 Hz), 2.40 (s), 2.22 (s). EI-MS: m/z 924 (100%) $[M - CO]^+$, 882 (10%) $[M - CO - {}^iPr]^+$. Anal. Found (Calcd for $C_{53}H_{92}OSi_4Ti_2$): C, 66.78 (66.77); H, 9.81 (9.73) %. IR (NaCl): **7** 1655 (br, ν(CO)); [^{13}C]**7** 1616 (br, $\nu(^{13}CO)$) cm^{-1}.

*$Ti_2(\mu{:}\eta^5,\eta^5\text{-}Pn^\dagger)_2(\mu{:}\eta^2,\eta^2\text{-}CS_2)$ (**8**).* To a solution of **1** (58 mg, 0.058 mmol) in pentane (2 mL) at −35 °C was added CS_2 (14 μL, 0.23 mmol) via microsyringe. The resultant dark-green mixture was allowed to warm to room temperature and stir for 3 h. Filtration followed by cooling to −35 °C afforded red microcrystals that were isolated by decantation and dried in vacuo. Total yield: 36 mg (62% with respect to **1**). Recrystallization from a saturated Et_2O solution at −35 °C afforded dark-red crystals suitable for X-ray diffraction studies. Alternatively, recrystallization from a saturated $SiMe_4$ solution at −35 °C afforded red crystals with different unit cell parameters (see Table S1 in the Supporting Information). ^{1}H NMR (toluene-d_8, 399.5 MHz, 303 K): δ_H 7.30 (2H, $^3J_{HH}$ = 3.0 Hz, Pn *H*), 6.35 (2H, $^3J_{HH}$ = 3.0 Hz, Pn *H*), 6.25 (2H, $^3J_{HH}$ = 3.5 Hz, Pn *H*), 5.85 (2H, $^3J_{HH}$ = 3.5 Hz, Pn *H*), 1.48 (6H, m, ^{i}Pr C*H*), 1.42 (6H, m, ^{i}Pr C*H*), 1.15 (18H, d, $^3J_{HH}$ = 7.4 Hz, ^{i}Pr CH_3), 1.13 (18H, d, $^3J_{HH}$ = 7.5 Hz, ^{i}Pr CH_3), 1.05 (18H, d, $^3J_{HH}$ = 7.4 Hz, ^{i}Pr CH_3), 1.01 (18H, d, $^3J_{HH}$ = 7.5 Hz, ^{i}Pr CH_3). ^{13}C{^{1}H} NMR (toluene-d_8, 100.5 MHz, 303 K): δ_C 355.5 (CS_2), 133.4 (Pn *C*), 132.4 (Pn C), 127.1 (Pn *C*), 107.6 (Pn *C*), 105.5 (Pn *C*), 95.1 (Pn *C*), 20.37 (^{i}Pr CH_3), 20.21 (^{i}Pr CH_3), 19.82 (^{i}Pr CH_3), 14.73 (^{i}Pr CH), 12.93 (^{i}Pr CH). ^{29}Si{^{1}H} NMR (toluene-d_8, 79.4 MHz, 303 K): δ_{Si} 7.65, 7.39. EI-MS: m/z 1002 (65%) $[M]^+$, 960 (30%) $[M - {}^iPr]^+$. Anal. Found (Calcd for $C_{53}H_{92}S_2Si_4Ti_2$): C, 63.49 (63.56); H, 9.26 (9.26) %. IR (methylcyclohexane, 26 °C): 1104 (ν_{asym}(SCS)) cm^{-1}.

*$Ti_2(\mu{:}\eta^5,\eta^5\text{-}Pn^\dagger)_2COS$ (**9**).* A J. Young NMR tube was charged with **1** (20 mg, 0.022 mmol) and methylcyclohexane-d_{14} (0.6 mL), and the solution was cooled to −78 °C. The headspace was evacuated, and COS (0.048 mmol) was admitted. The tube was briefly shaken, and a color change from deep red to green was observed. NMR spectra were immediately measured, with the probe precooled to −30 °C. NMR yield: 45% with respect to **1**. ^{1}H NMR (methylcyclohexane-d_{14}, 399.5 MHz, 243 K, selected data): δ_H 7.00 (1H, d, $^3J_{HH}$ = 3.0 Hz, Pn *H*), 6.96 (1H, d, $^3J_{HH}$ = 3.0 Hz, Pn *H*), 6.72 (1H, d, $^3J_{HH}$ = 3.7 Hz, Pn *H*), 6.45 (1H, d, $^3J_{HH}$ = 3.0 Hz, Pn *H*), 6.43 (1H, d, $^3J_{HH}$ = 3.6 Hz, Pn *H*), 6.31 (1H, d, $^3J_{HH}$ = 3.7 Hz, Pn *H*), 6.09 (1H, d, $^3J_{HH}$ = 3.7 Hz, Pn *H*), 1.79−1.44 (12H, overlapping m, ^{i}Pr C*H*), 1.34−1.02 (72H, overlapping m, ^{i}Pr CH_3). One Pn *H* signal was not resolved because of coincidental overlap with signals of **12**. ^{13}C{^{1}H} NMR (methylcyclohexane-d_{14}, 100.5 MHz, 243 K, selected data): δ_C 283 (s, COS). ^{29}Si{^{1}H} NMR (methylcyclohexane-d_{14}, 79.4 MHz, 243 K, selected data): δ_{Si} 2.48, 2.07, 1.73, 1.08. IR (NaCl): 1493 (ν_{asym}(SCO)) cm^{-1}. IR (methylcyclohexane, −65 °C): 1498 (ν_{asym}(SCO)) cm^{-1}. EI-MS and microanalysis data were not obtained for **9** because of its susceptibility to further reaction above −40 °C.

*$Ti_2(\mu{:}\eta^5,\eta^5\text{-}Pn^\dagger)_2S(CO)$ (**10**).* Method A: A J. Young NMR tube charged with **1** (16 mg, 0.017 mmol) and toluene-d_8 (0.65 mL) at −78 °C was degassed, and COS gas (0.015 mmol) was slowly admitted. The reaction mixture was briefly shaken, resulting in a color change from deep red to green, and the mixture was allowed to warm to room temperature over a period of 2 h. NMR yield: 47% with respect to **1**. Method B: An ampule charged with **11** (0.028 mmol) and toluene-d_8 (0.7 mL) was cooled to −78 °C, and the headspace was evacuated. ^{13}CO gas (0.025 mmol) was slowly admitted to the stirred mixture, resulting in a color change from red to green. The solution was warmed to room temperature and then decanted into a J. Young tube, and [^{13}C]**10** was identified by its NMR and IR spectra. NMR yield: 75% with respect to **1**. Alternatively, exposing a solution of **11** to 0.9 molar equiv of CO via Toepler pump yielded primarily the unlabeled product **10**. ^{1}H NMR (toluene-d_8, 399.5 MHz, 303 K, selected data): δ_H 7.81 (2H, d, $^3J_{HH}$ = 2.9 Hz, Pn *H*), 6.09 (br, $\Delta\nu_{1/2}$ = 13 Hz, Pn *H*), 5.75 (2H, d, $^3J_{HH}$ = 2.9 Hz, Pn *H*), 5.38 (2H, d, $^3J_{HH}$ = 2.7 Hz, Pn *H*), 1.62−1.24 (12H, overlapping m, ^{i}Pr C*H*), 1.22−0.96 (72H, overlapping m, ^{i}Pr CH_3). ^{13}C{^{1}H} NMR (toluene-d_8, 100.5 MHz, 303 K, selected data): δ_C 247 (br, $\Delta\nu_{1/2}$ = 110 Hz, CO). ^{29}Si{^{1}H} NMR (toluene-d_8, 79.4 MHz, 303 K, selected data): δ_{Si} 2.56, 1.46. IR (methylcyclohexane, −65 °C): **10** 2011 (br, ν(CO)); [^{13}C]**10** 1966 (br, $\nu(^{13}CO)$) cm^{-1}. EI-MS and microanalysis data were not obtained for **10** because of its susceptibility to further reaction above −40 °C.

*$Ti_2(\mu{:}\eta^5,\eta^5\text{-}Pn^\dagger)_2(\mu\text{-}S)$ (**11**).* A solution of Ph_3PS (56 mg, 0.19 mmol) in toluene (3 mL) was added dropwise to a stirred solution of **1** (177 mg, 0.191 mmol) in pentane (3 mL) at −35 °C. The resultant red mixture was allowed to warm to room temperature, stirred for 30 min, and then stripped to dryness. A red residue was obtained, which was placed under high vacuum (ca. 10^{-6} mbar) and heated at 75 °C for 1 h and then 100 °C for 2 h to ensure complete sublimation of a white crystalline solid, presumably Ph_3P. The residue was extracted with pentane (3 × 2 mL), filtered, and allowed to concentrate to ca. 3 mL. Cooling of this solution to −35 °C afforded red crystals of **11** suitable for X-ray diffraction studies. Total yield: 95 mg (52% with respect to **1**). ^{1}H NMR (C_6D_6, 399.5 MHz, 303 K): δ_H 9.25 (2H, d, $^3J_{HH}$ = 3.4 Hz, Pn *H*), 7.06 (2H, d, $^3J_{HH}$ = 3.2 Hz, Pn *H*), 6.10 (2H, d, $^3J_{HH}$ = 3.1 Hz, Pn *H*), 5.96 (2H, d, $^3J_{HH}$ = 3.4 Hz, Pn *H*), 2.01 (6H, m, ^{i}Pr C*H*), 1.35 (6H, m, ^{i}Pr C*H*), 1.17 (18H, d, $^3J_{HH}$ = 7.5 Hz, ^{i}Pr CH_3), 1.13 (18H, d, $^3J_{HH}$ = 7.3 Hz, ^{i}Pr CH_3), 0.98 (18H, d, $^3J_{HH}$ = 7.5 Hz, ^{i}Pr CH_3), 0.60 (18H, d, $^3J_{HH}$ = 7.5 Hz, ^{i}Pr CH_3). ^{13}C{^{1}H} NMR (C_6D_6, 100.5 MHz, 303 K): δ_C 141.7 (Pn *C*), 132.5 (Pn *C*), 130.0 (Pn *C*), 123.0 (Pn C), 118.6 (Pn *C*), 115.3 (Pn C), 113.2 (Pn C), 98.53 (Pn *C*), 19.50 (^{i}Pr CH_3), 19.41 (^{i}Pr CH_3), 19.14 (^{i}Pr CH_3), 18.89 (^{i}Pr CH_3), 13.72 (^{i}Pr CH), 13.15 (^{i}Pr CH). ^{29}Si{^{1}H} NMR (C_6D_6, 79.4 MHz, 303 K): δ_{Si} 2.20, 1.82. EI-MS: m/z 989 (60%) $[M + S]^+$, 956−959 (principal peak 957, 20%) $[M]^+$, 877 (100%) $[M - Ti - S]^+$. Anal. Found (Calcd for $C_{52}H_{92}SSi_4Ti_2$): C, 65.33 (65.23); H, 9.61 (9.69) %.

*$[(\eta^8\text{-}Pn^\dagger)Ti(\mu\text{-}S)]_2$ (**12**).* Method A: An ampule containing a solution of **1** (141 mg, 0.152 mmol) in benzene (2 mL), frozen at −35 °C, was degassed and fitted with a balloon containing COS gas (1 atm). The solution was allowed to warm to room temperature and, shortly after thawing, appeared green in color. After 30 min of stirring at room temperature, a color change to red-brown was observed. The reaction mixture was frozen and lyophilized, and a spectroscopically pure red-brown solid was isolated. Total yield: 145 mg (96% with respect to **1**). Method B: To an ampule containing **1** (100 mg, 0.108 mmol) and Ph_3PS (64 mg, 0.216 mmol) was added toluene (2 mL). After 4 h of stirring at room temperature, the red-brown mixture was stripped to dryness, extracted with Et_2O (2 × 5 mL), and filtered, and the solvent was removed in vacuo. A brown solid was obtained, which was placed under high vacuum (ca. 10^{-6} mbar) and heated at 60 °C for 2.5 h, 75 °C for 1 h, and finally 100 °C for 30 min to ensure complete sublimation of a white crystalline solid, presumably Ph_3P. The residue was extracted with Et_2O (2 × 5 mL), filtered, and allowed to concentrate to ca. 4 mL. Cooling of this solution to −35 °C afforded red crystals suitable for X-ray diffraction studies. Total yield: 86 mg (80% with respect to **1**). ^{1}H NMR (C_6D_6, 399.5 MHz, 303 K): δ_H 6.59 (4H, d, $^3J_{HH}$ = 3.3 Hz, Pn H), 5.92 (4H, d, $^3J_{HH}$ = 3.2 Hz, Pn H), 1.31 (12H, m, ^{i}Pr CH), 1.19 (36H, d, $^3J_{HH}$ = 7.3 Hz, ^{i}Pr CH_3), 1.14 (36H, d, $^3J_{HH}$ = 7.3 Hz, ^{i}Pr CH_3). ^{13}C{^{1}H} NMR (C_6D_6, 100.5 MHz, 303 K): δ_C 148.9 (Pn C), 130.0 (Pn C), 115.2 (Pn C), 113.9 (Pn C), 19.66 (^{i}Pr CH_3), 19.50 (^{i}Pr CH_3), 12.31 (^{i}Pr CH). ^{29}Si{^{1}H} NMR (C_6D_6, 79.4 MHz, 303 K): δ_{Si} −0.15. EI-MS: m/z 989 (100%) $[M]^+$, 946 (50%) $[M - {}^iPr]^+$. Anal. Found (Calcd for $C_{52}H_{92}S_2Si_4Ti_2$): C, 63.20 (63.12); H, 9.44 (9.37) %.

Kinetic Studies. Decomposition rates of **4** at seven temperatures between 9 to 40 °C were measured by the same method: A J. Young NMR tube was charged with 0.50 mL of a stock solution containing **1** (0.0295 M, 0.015 mmol) and ferrocene (0.0935 M) in methylcyclohexane-d_{14}, and the solution was cooled to −78 °C. The headspace was evacuated, and $^{13}CO_2$ (0.015 mmol) was admitted. The tube was briefly shaken, and a color change from deep red to dark green was observed. After 30 min the tube was removed from the −78 °C bath, placed in a pre-equilibrated VT-NMR probe, and shimmed as thermal equilibrium was attained (10 min). To avoid any complications due to different relaxation times for the resonances, spectra were recorded using one 90° pulse. ^{1}H spectra were acquired periodically (33.6 s repetition time), and the time of each spectrum was recorded along with the data by the internal clock on the

DOI: 10.1021/acs.organomet.5b00315
Organometallics 2015, 34, 4816−4829

spectrometer. A baseline correction was applied, and the concentrations of **4** were determined by integration over the same region of each spectrum relative to the ferrocene resonance. The temperature in the probe was calibrated by measuring the peak separation of a sample of neat methanol.[83] Concentration versus time data were analyzed by fitting the data for **4** to a first-order exponential decay. Plots of ln([**4**]) versus time and the derived rate constants are included in the Supporting Information. The activation parameters were calculated from a linear fit of the Eyring plot, $\ln(k_{obs}/T)$ versus $1/T$. The error in the determination of the activation parameters was calculated according to Girolami and co-workers.[84]

Crystallographic Details. Single-crystal XRD data for **7**, **8** ($SiMe_4$), **11**, and **12** were collected by the U.K. National Crystallography Service (NCS)[85] at the University of Southampton on a Rigaku FR-E+ Ultra High Flux diffractometer ($\lambda_{Mo\ K\alpha}$) equipped with VariMax VHF optics and a Saturn 724+ CCD area detector. The data were collected at 100 or 150 K using an Oxford Cryosystems Cobra low-temperature device. Data collected by the NCS were processed using CrystalClear-SM Expert 3.1 b18,[86] and unit cell parameters were refined against all data. Single-crystal XRD data for **5** and **8** (Et_2O) were collected at the University of Sussex on a Enraf-Nonius CAD4 diffractometer with graphite-monochromatized ($\lambda_{Mo\ K\alpha}$) radiation or an Agilent Technologies Xcalibur Gemini Ultra diffractometer ($\lambda_{Mo\ K\alpha}$ or $\lambda_{Cu\ K\alpha}$ source) equipped with an Eos CCD area detector. The data were collected at 173 K using an Oxford Cryosystems Cobra low-temperature device. Data were processed using KappaCCD software or CrysAlisPro (version 1.171.36.32),[87] and unit cell parameters were refined against all data. An empirical absorption correction was carried out using the Multi-Scan program.[88] All of the structures were solved using SHELXL-2013,[89] DIRDIF-2008,[90] or SUPERFLIP[91] and refined on F_o^2 by full-matrix least-squares refinements using SHELXL-2013.[89] Solutions and refinements were performed using the OLEX2[92] or WinGX[93] packages and software packages within. All non-hydrogen atoms were refined with anisotropic displacement parameters. All hydrogen atoms were refined using a riding model. Disordered solvent molecules in **8** (Et_2O) and **12** could not be modeled properly; therefore, this disorder was treated using the SQUEEZE[94] routine in PLATON.[95] Disordered solvent molecules in **11** were treated using the solvent mask routine in OLEX2,[92] which resulted in improved refinement indices relative to SQUEEZE, so these data have been included.

Computational Details. DFT calculations were carried out using two computational methods. One employed the Amsterdam Density Functional package (version ADF2012.01).[96] The Slater-type orbital (STO) basis sets were of triple-ζ quality augmented with one polarization function (ADF basis TZP). Core electrons were frozen (C 1s; Ti 2p) in the model of the electronic configuration for each atom. The local density approximation (LDA) of Vosko, Wilk, and Nusair (VWN)[97] was used together with the exchange−correlation corrections of Becke and Perdew (BP86).[98,99] The other used Gaussian 09, revision A.02,[100] with the B3LYP functional and SDD basis set. In both sets of calculations, tight optimization conditions were used and frequency calculations were used to confirm stationary points.

■ ASSOCIATED CONTENT

Supporting Information

Additional NMR spectroscopic, X-ray crystallographic, and kinetic data; a text file of all computed molecule Cartesian coordinates in .xyz format for convenient visualization; crystallographic data in CIF format. The Supporting Information is available free of charge on the ACS Publications website at DOI: 10.1021/acs.organomet.5b00315.

■ AUTHOR INFORMATION

Corresponding Authors

*E-mail for F.G.N.C.: f.g.cloke@sussex.ac.uk.

*E-mail for J.C.G.: jennifer.green@chem.ox.ac.uk.

Notes

The authors declare no competing financial interest.

■ ACKNOWLEDGMENTS

We thank the European Research Council and the University of Sussex for financial support. Dr. S. M. Roe (Sussex), Dr. B. M. Day (Manchester), and NCS Southampton are thanked for their assistance with X-ray crystallography.

■ REFERENCES

(1) IPCC. *Climate Change 2013: The Physical Science Basis*; Stocker, T. F., Qin, D., Plattner, G.-K., Tignor, M. M. B., Allen, S. K., Boschung, J., Nauels, A., Xia, Y., Bex, V., Midgley, P. M., Eds.; Working Group I Contribution to the Fifth Assessment Report of the Intergovernmental Panel on Climate Change, Summary for Policymakers, 2013.

(2) *Carbon Dioxide as Chemical Feedstock*; Aresta, M., Ed.; Wiley-VCH: Weinheim, Germany, 2010.

(3) Sakakura, T.; Choi, J.-C.; Yasuda, H. *Chem. Rev.* **2007**, *107*, 2365−2387.

(4) Arakawa, H.; Aresta, M.; Armor, J. N.; Barteau, M. A.; Beckman, E. J.; Bell, A. T.; Bercaw, J. E.; Creutz, C.; Dinjus, E.; Dixon, D. A.; et al. *Chem. Rev.* **2001**, *101*, 953−996.

(5) West, N. M.; Miller, A. J.; Labinger, J. A.; Bercaw, J. E. *Coord. Chem. Rev.* **2011**, *255*, 881−898.

(6) Williams, V. A.; Manke, D. R.; Wolczanski, P. T.; Cundari, T. R. *Inorg. Chim. Acta* **2011**, *369*, 203−214.

(7) Cokoja, M.; Bruckmeier, C.; Rieger, B.; Herrmann, W. A.; Kühn, F. E. *Angew. Chem., Int. Ed.* **2011**, *50*, 8510−8537.

(8) Yin, X.; Moss, J. R. *Coord. Chem. Rev.* **1999**, *181*, 27−59.

(9) Leitner, W. *Coord. Chem. Rev.* **1996**, *153*, 257−284.

(10) Gibson, D. H. *Chem. Rev.* **1996**, *96*, 2063−2096.

(11) Lu, Z.; Wang, Y.; Liu, J.; Lin, Y.-J.; Li, Z. H.; Wang, H. *Organometallics* **2013**, *32*, 6753−6758.

(12) Ashley, A.; O'Hare, D. *Top. Curr. Chem.* **2013**, *334*, 191−217.

(13) Mömming, C. M.; Otten, E.; Kehr, G.; Fröhlich, R.; Grimme, S.; Stephan, D. W.; Erker, G. *Angew. Chem., Int. Ed.* **2009**, *48*, 6643−6646.

(14) Evans, W. J.; Perotti, J. M.; Brady, J. C.; Ziller, J. W. *J. Am. Chem. Soc.* **2003**, *125*, 5204−5212.

(15) Evans, W. J.; Seibel, C. A.; Ziller, J. W. *Inorg. Chem.* **1998**, *37*, 770−776.

(16) Lam, O. P.; Meyer, K. *Polyhedron* **2012**, *32*, 1−9.

(17) Gardner, B. M.; Liddle, S. T. *Eur. J. Inorg. Chem.* **2013**, 3753−3770.

(18) La Pierre, H. S.; Meyer, K. *Prog. Inorg. Chem.* **2014**, *58*, 303−416.

(19) Berthet, J.-C.; Le Maréchal, J.-F.; Nierlich, M.; Lance, M.; Vigner, J.; Ephritikhine, M. *J. Organomet. Chem.* **1991**, *408*, 335−341.

(20) Brennan, J. G.; Andersen, R. A.; Zalkin, A. *Inorg. Chem.* **1986**, *25*, 1761−1765.

(21) Castro, L.; Labouille, S.; Kindra, D. R.; Ziller, J. W.; Nief, F.; Evans, W. J.; Maron, L. *Chem.—Eur. J.* **2012**, *18*, 7886−7895.

(22) Castro, L.; Lam, O. P.; Bart, S. C.; Meyer, K.; Maron, L. *Organometallics* **2010**, *29*, 5504−5510.

(23) Castro, L.; Maron, L. *Chem.—Eur. J.* **2012**, *18*, 6610−6615.

(24) Castro-Rodriguez, I.; Nakai, H.; Zakharov, L. N.; Rheingold, A. L.; Meyer, K. *Science* **2004**, *305*, 1757−1759.

(25) Tsoureas, N.; Castro, L.; Kilpatrick, A. F. R.; Maron, L.; Cloke, F. G. N. *Chem. Sci.* **2014**, *5*, 3777−3788.

(26) Laitar, D. S.; Müller, P.; Sadighi, J. P. *J. Am. Chem. Soc.* **2005**, *127*, 17196−17197.

(27) Chirik, P. J. *Organometallics* **2010**, *29*, 1500−1517.

(28) Chirik, P. J.; Bouwkamp, M. W. In *Comprehensive Organometallic Chemistry III*; Mingos, D. M. P., Crabtree, R. H., Eds.; Elsevier: Oxford, U.K., 2007; pp 243−279.

(29) Alt, H. G.; Schwind, K.-H.; Rausch, M. D. *J. Organomet. Chem.* **1987**, *321*, C9−C12.

(30) Demerseman, B.; Mah, R.; Dixneuf, P. H. *J. Chem. Soc., Chem. Commun.* **1984**, 1394−1396.

DOI: 10.1021/acs.organomet.5b00315
Organometallics 2015, 34, 4816−4829

(31) Burlakov, V. V.; Polyakov, A. V.; Yanovsky, A. I.; Struchkov, Y. T.; Shur, V. B.; Vol'pin, M. E.; Rosenthal, U.; Görls, H. *J. Organomet. Chem.* **1994**, *476*, 197−206.
(32) Lefeber, C.; Ohff, A.; Tillack, A.; Baumann, W.; Kempe, R.; Burlakov, V. V.; Rosenthal, U.; Görls, H. *J. Organomet. Chem.* **1995**, *501*, 179−188.
(33) Burlakov, V. V.; Yanovsky, A. I.; Struchkov, Y. T.; Rosenthal, U.; Spannenberg, A.; Kempe, R.; Ellert, O. G.; Shur, V. B. *J. Organomet. Chem.* **1997**, *542*, 105−112.
(34) Burlakov, V. V.; Rosenthal, U.; Dolgushin, F. M.; Yanovsky, A. I.; Struchkov, Y. T.; Ellert, O. G.; Shur, V. B.; Vol'pin, M. E. *Metalloorg. Khim.* **1992**, *5*, 1231.
(35) Pellny, P.-M.; Burlakov, V. V.; Baumann, W.; Spannenberg, A.; Rosenthal, U. *Z. Anorg. Allg. Chem.* **1999**, *625*, 910−918.
(36) Fachinetti, G.; Floriani, C.; Chiesi-Villa, A.; Guastini, C. *J. Am. Chem. Soc.* **1979**, *101*, 1767−1775.
(37) Bottomley, F.; Lin, I. J. B.; Mukaida, M. *J. Am. Chem. Soc.* **1980**, *102*, 5238−5242.
(38) Burlakov, V. V.; Dolgushin, F. M.; Yanovsky, A. I.; Struchkov, Yu. T.; Shur, V. B.; Rosenthal, U.; Thewalt, U. *J. Organomet. Chem.* **1996**, *522*, 241−247.
(39) Santamaría, D.; Cano, J.; Royo, P.; Mosquera, M. E. G.; Cuenca, T.; Frutos, L. M.; Castaño, O. *Angew. Chem., Int. Ed.* **2005**, *44*, 5828−5830.
(40) Fröhlich, H.-O.; Schreer, H. *Z. Chem.* **1983**, *23*, 348−349.
(41) Cotton, F. A.; Murillo, C. A.; Walton, R. A. In *Multiple Bonds between Metal Atoms*, 3rd ed.; Walton, R. A., Ed.; Clarendon Press: Oxford, U.K., 2005.
(42) Lalrempuia, R.; Stasch, A.; Jones, C. *Chem. Sci.* **2013**, *4*, 4383−4388.
(43) Noor, A.; Qayyum, S.; Bauer, T.; Schwarz, S.; Weber, B.; Kempe, R. *Chem. Commun.* **2014**, *50*, 13127−13130.
(44) Palit, C. M.; Graham, D. J.; Chen, C.-H.; Foxman, B. M.; Ozerov, O. V. *Chem. Commun.* **2014**, *50*, 12840−12842.
(45) Krogman, J. P.; Foxman, B. M.; Thomas, C. M. *J. Am. Chem. Soc.* **2011**, *133*, 14582−14585.
(46) Summerscales, O. T.; Cloke, F. G. N. *Coord. Chem. Rev.* **2006**, *250*, 1122−1140.
(47) Katz, T. J.; Acton, N. *J. Am. Chem. Soc.* **1972**, *94*, 3281−3283.
(48) Katz, T. J.; Acton, N.; McGinnis, J. *J. Am. Chem. Soc.* **1972**, *94*, 6205−6206.
(49) Kuchta, M.; Cloke, F. G. N. *Organometallics* **1998**, *17*, 1934−1936.
(50) Balazs, G.; Cloke, F. G. N.; Harrison, A.; Hitchcock, P. B.; Green, J.; Summerscales, O. T. *Chem. Commun.* **2007**, 873−875.
(51) Balazs, G.; Cloke, F. G. N.; Gagliardi, L.; Green, J. C.; Harrison, A.; Hitchcock, P. B.; Shahi, A. R. M.; Summerscales, O. T. *Organometallics* **2008**, *27*, 2013−2020.
(52) Summerscales, O. T.; Rivers, C. J.; Taylor, M. J.; Hitchcock, P. B.; Green, J. C.; Cloke, F. G. N. *Organometallics* **2012**, *31*, 8613−8617.
(53) Ashley, A. E.; Cooper, R. T.; Wildgoose, G. G.; Green, J. C.; O'Hare, D. *J. Am. Chem. Soc.* **2008**, *130*, 15662−15677.
(54) Kilpatrick, A. F. R.; Green, J. C.; Cloke, F. G. N.; Tsoureas, N. *Chem. Commun.* **2013**, *49*, 9434−9436.
(55) Kilpatrick, A. F. R.; Cloke, F. G. N. *Chem. Commun.* **2014**, *50*, 2769−2771.
(56) Kilpatrick, A. F. R.; Green, J. C.; Cloke, F. G. N. *Organometallics* **2015**, DOI: 10.1021/acs.organomet.5b00363.
(57) Jegat, C.; Fouassier, M.; Tranquille, M.; Mascetti, J. *Inorg. Chem.* **1991**, *30*, 1529−1536.
(58) Evans, J. *J. Chem. Soc.* **1959**, 2003−2005.
(59) Schubert, E. M. *J. Chem. Educ.* **1992**, *69*, 62.
(60) Werner, H. *Coord. Chem. Rev.* **1982**, *43*, 165−185.
(61) Pandey, K. K. *Coord. Chem. Rev.* **1997**, *140*, 37−114.
(62) Herzberg, G. *Electronic Spectra and Electronic Structure of Polyatomic Molecules*; Molecular Spectra and Molecular Structure, Vol. 3; Van Nostrand-Reinhold: New York, 1966.
(63) Eland, J. H. D.; Berkowitz, J. *J. Chem. Phys.* **1979**, *70*, 5151−5156.
(64) Cox, J. D.; Wagman, D. D.; Medvedev, V. A. *CODATA Key Values for Thermodynamics*; Hemisphere: New York, 1989.
(65) *CRC Handbook of Chemistry and Physics*, 80th ed.; Lide, D. R., Ed.; CRC Press: Boca Raton, FL, 1999.
(66) Pinkas, J.; Císařová, I.; Horáček, M.; Kubišta, J.; Mach, K. *Organometallics* **2011**, *30*, 1034−1045.
(67) Gibson, D. H.; Ye, M.; Richardson, J. F. *J. Am. Chem. Soc.* **1992**, *114*, 9716−9717.
(68) Gibson, D. H.; Mehta, J. M.; Ye, M.; Richardson, J. F.; Mashuta, M. S. *Organometallics* **1994**, *13*, 1070−1072.
(69) Aresta, M.; Dibenedetto, A. *Dalton Trans.* **2007**, 2975−2992.
(70) Lee, C. H.; Laitar, D. S.; Mueller, P.; Sadighi, J. P. *J. Am. Chem. Soc.* **2007**, *129*, 13802−13803.
(71) Nakamoto, K. *Infrared and Raman Spectra of Inorganic and Coordination Compounds, Part A*, 6th ed.; Wiley: Hoboken, NJ, 2009.
(72) Haack, P.; Limberg, C.; Tietz, T.; Metzinger, R. *Chem. Commun.* **2011**, *47*, 6374−6376.
(73) Fischer, P. J.; Young, V. G., Jr.; Ellis, J. E. *Chem. Commun.* **1997**, 1249−1250.
(74) Dick, D. G.; Hou, Z.; Stephan, D. W. *Organometallics* **1992**, *11*, 2378−2382.
(75) Barr, R. D.; Green, M.; Howard, J. A. K.; Marder, T. B.; Moore, I.; Stone, F. G. A. *J. Chem. Soc., Chem. Commun.* **1983**, 746−748.
(76) Awang, M. R.; Barr, R. D.; Green, M.; Howard, J. A. K.; Marder, T. B.; Stone, F. G. A. *J. Chem. Soc., Dalton Trans.* **1985**, 2009.
(77) Dawkins, G. M.; Green, M.; Mead, K. A.; Salaün, J.-Y.; Stone, F. G. A.; Woodward, P. *J. Chem. Soc., Dalton Trans.* **1983**, 527−530.
(78) Horwitz, C. P.; Shriver, D. F. *Adv. Organomet. Chem.* **1984**, *23*, 219−305.
(79) NIST. Diatomic Spectral Database. http://www.nist.gov/pml/data/msd-di/index.cfm (accessed Sept 18, 2014).
(80) Merola, J. S.; Gentile, R. A.; Ansell, G. B.; Modrick, M.; Zentz, S. *Organometallics* **1982**, *1*, 1731−1733.
(81) Hamilton, D. M.; Willis, W. S.; Stucky, G. D. *J. Am. Chem. Soc.* **1981**, *103*, 4255−4256.
(82) Brisdon, A. K. *Inorganic Spectroscopic Methods*; Oxford Chemistry Primers, Vol. *62*; Oxford University Press: Oxford, U.K., 1998.
(83) Ammann, C.; Meier, P.; Merbach, A. E. *J. Magn. Reson.* **1982**, *46*, 319−321.
(84) Morse, P. M.; Spencer, M. D.; Wilson, S. R.; Girolami, G. S. *Organometallics* **1994**, *13*, 1646−1655.
(85) Coles, S. J.; Gale, P. A. *Chem. Sci.* **2012**, *3*, 683−689.
(86) *CrystalClear*; Rigaku: Tokyo, 2011.
(87) *CrysalisPro*, version 1.171.36.32; Agilent Technologies: Santa Clara, CA, 2011.
(88) Blessing, R. H. *Acta Crystallogr., Sect. A* **1995**, *51*, 33−38.
(89) Sheldrick, G. M. *Acta Crystallogr., Sect. A* **2008**, *64*, 112−122.
(90) Beurskens, P. T.; Beurskens, G.; Gelder, R.; Smits, J. M. M.; LGarcia-Granda, S.; Gould, R. O. *DIRDIF-2008*, 2008.
(91) Palatinus, L.; Chapuis, G. *J. Appl. Crystallogr.* **2007**, *40*, 786−790.
(92) Dolomanov, O. V.; Bourhis, L. J.; Gildea, R. J.; Howard, J. A. K.; Puschmann, H. *J. Appl. Crystallogr.* **2009**, *42*, 339−341.
(93) Farrugia, L. J. *J. Appl. Crystallogr.* **1999**, *32*, 837−838.
(94) van der Sluis, P.; Spek, A. L. *Acta Crystallogr., Sect. A* **1990**, *46*, 194−201.
(95) Spek, A. L. *J. Appl. Crystallogr.* **2003**, *36*, 7−13.
(96) *Amsterdam Density Functional (ADF) Modeling Suite*; Scientific Computing & Modelling NV: Amsterdam, 2006.
(97) Vosko, S. H.; Wilk, L.; Nusair, M. *Can. J. Phys.* **1980**, *58*, 1200−1211.
(98) Becke, A. *Phys. Rev. A* **1988**, *38*, 3098−3100.
(99) Perdew, J. P. *Phys. Rev. B* **1986**, *33*, 8822−8824.
(100) Frisch, M. J.; Trucks, G. W.; Schlegel, H. B.; Scuseria, G. E.; Robb, M. A.; Cheeseman, J. R.; Scalmani, G.; Barone, V.; Mennucci, B.; Petersson, G. A.; Nakatsuji, H.; Caricato, M.; Li, X.; Hratchian, H. P.; Izmaylov, A. F.; Bloino, J.; Zheng, G.; Sonnenberg, J. L.; Hada, M.; Ehara, M.; Toyota, K.; Fukuda, R.; Hasegawa, J.; Ishida, M.; Nakajima,

DOI: 10.1021/acs.organomet.5b00315
Organometallics 2015, 34, 4816−4829

T.; Honda, Y.; Kitao, O.; Nakai, H.; Vreven, T.; Montgomery, J. A., Jr.; Peralta, J. E.; Ogliaro, F.; Bearpark, M.; Heyd, J. J.; Brothers, E.; Kudin, K. N.; Staroverov, V. N.; Kobayashi, R.; Normand, J.; Raghavachari, K.; Rendell, A.; Burant, J. C.; Iyengar, S. S.; Tomasi, J.; Cossi, M.; Rega, N.; Millam, J. M.; Klene, M.; Knox, J. E.; Cross, J. B.; Bakken, V.; Adamo, C.; Jaramillo, J.; Gomperts, R.; Stratmann, R. E.; Yazyev, O.; Austin, A. J.; Cammi, R.; Pomelli, C.; Ochterski, J. W.; Martin, R. L.; Morokuma, K.; Zakrzewski, V. G.; Voth, G. A.; Salvador, P.; Dannenberg, J. J.; Dapprich, S.; Daniels, A. D.; Farkas, Ö.; Foresman, J. B.; Ortiz, J. V.; Cioslowski, J.; Fox, D. J. *Gaussian 09*, revision A.02; Gaussian, Inc.: Wallingford, CT, 2009.

DOI: 10.1021/acs.organomet.5b00315
Organometallics 2015, 34, 4816−4829